Article

Current Biology

Balancing limited resources in actin network competition

Graphical abstract

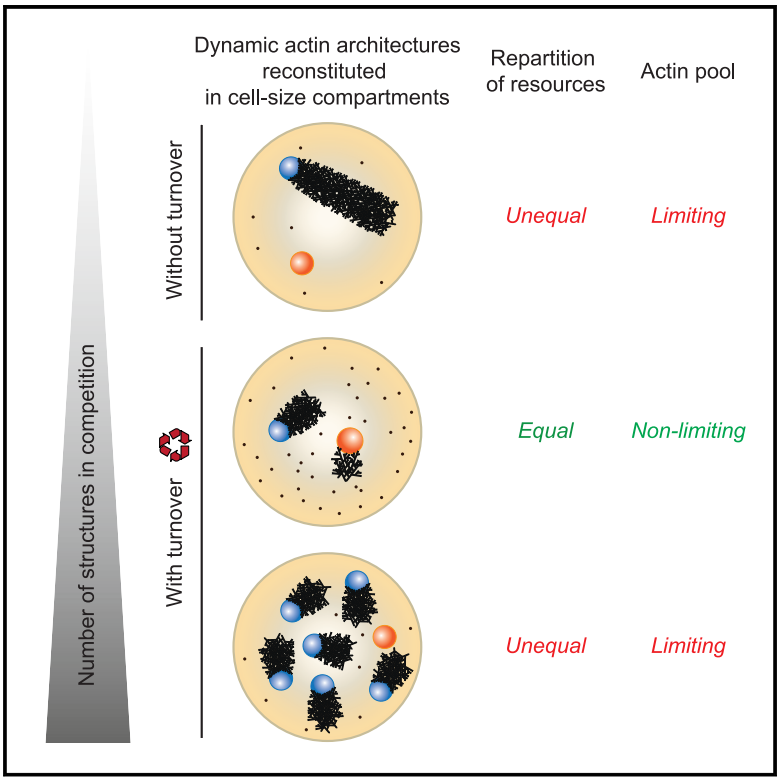

Highlights

- Size of non-dynamic actin structures is defined by the limiting pool of components
- Actin turnover maintains a high pool of monomers available for architecture growth
- Protein turnover allows the coexistence of actin structures with various densities
- If competition level is too high, turnover cannot maintain all the architectures

Authors

Christophe Guérin, Anne-Betty N'Diaye, Laurène Gressin, Alex Mogilner, Manuel Théry, Laurent Blanchoin, Alexandra Colin

Correspondence

manuel.thery@cea.fr (M.T.), laurent.blanchoin@cnrs.fr (L.B.), alexandra.colin@cnrs.fr (A.C.)

In brief

Guérin et al. use actin-based motility in closed microwells to study how a limited amount of proteins is shared between competitive architectures. They show the importance of turnover for the coexistence of actin networks with various densities. With too many structures in competition, turnover is not sufficient to maintain all the architectures.

Guérin et al., 2025, Current Biology *35*, 500–513
February 3, 2025
https://doi.org/10.1016/j.cub.2024.11.067

CellPress

CellPress

Current Biology

Article

Balancing limited resources in actin network competition

Christophe Guérin,[1] Anne-Betty N'Diaye,[1] Laurène Gressin,[1] Alex Mogilner,[2] Manuel Théry,[3,*] Laurent Blanchoin,[1,3,*] and Alexandra Colin[1,4,5,*]

[1]Cytomorpholab, Laboratoire de Physiologie Cellulaire and Végétale, Interdisciplinary Research Institute of Grenoble, University of Grenoble-Alpes, CEA, CNRS, INRA, 17 avenue des Martyrs, 38054 Grenoble, France

[2]Courant Institute of Mathematical Sciences and Department of Biology, New York University, 251 Mercer Street, New York, NY 10012, USA

[3]Cytomorpholab, Institut Chimie Biologie Innovation, Institut Pierre-Gilles de Gennes, Université Paris Sciences et Lettres, CEA, ESPCI, 6 rue Jean Calvin, 75005 Paris, France

[4]X (formerly Twitter): @acoli12

[5]Lead contact

*Correspondence: manuel.thery@cea.fr (M.T.), laurent.blanchoin@cnrs.fr (L.B.), alexandra.colin@cnrs.fr (A.C.)

https://doi.org/10.1016/j.cub.2024.11.067

SUMMARY

In cells, multiple actin networks coexist in a dynamic manner. These networks compete for a common pool of actin monomers and actin-binding proteins. Interestingly, all of these networks manage to coexist despite the strong competition for resources. Moreover, the coexistence of networks with various strengths is key to cell adaptation to external changes. However, a comprehensive view of how these networks coexist in this competitive environment, where resources are limited, is still lacking. To address this question, we used a reconstituted system, in closed microwells, consisting of beads propelled by actin polymerization or micropatterns functionalized with lipids capable of initiating polymerization close to a membrane. This system enabled us to build dynamic actin architectures, competing for a limited pool of proteins, over a period of hours. We demonstrated the importance of protein turnover for the coexistence of actin networks, showing that it ensures resource distribution between weak and strong networks. However, when competition becomes too intense, turnover alone is insufficient, leading to a selection process that favors the strongest networks. Consequently, we emphasize the importance of competition strength, which is defined by the turnover rate, the amount of available protein, and the number of competing structures. More generally, this work illustrates how turnover allows biological populations with various competition strengths to coexist despite resource constraints.

INTRODUCTION

Competition for resources exists at all levels in nature. In ecological communities, the different species sharing the same habitat compete for food resources.[1,2] Competition for limited resources has been proposed to be a driver of evolution, but how to ensure a stable coexistence of various species sharing the same resources is still an open question in ecology.[3,4] In multicellular organisms, the organs compete for resources during development. Indeed, impeding the growth of one organ will often make the other organs bigger.[5,6] At a more microscopic level, inter-cellular competition has been proposed to be a surveillance mechanism for the detection and elimination of suboptimal cells during development.[7–9] In the tumoral context, cell competition was proposed to have two opposite effects: elimination of pre-tumoral cells or at later stages, promotion of tumor expansion.[10,11] In those models, the cells compete for resources (trophic factors in the ligand capture model) or for limited space (mechanical constraints). Finally, there is also competition within the cell, due to the finite pool of resources that leads to the budgeting of resources for cell decision-making.[12] Indeed, many proteins are shared between several signaling pathways or incorporated into different cellular architectures. This is particularly true for actin, one of the most abundant proteins in the cell, which plays a crucial role in various physiological functions, including maintaining cell architecture, facilitating cell movement, and enabling endocytosis.[13,14] In recent years, it has become widely accepted that the actin monomer pool is shared among various cellular structures and is limited, thereby influencing notably the size of actin structures (reviewed in Michelot and Drubin[15–19], Rotty and Bear[15–19], Suarez and Kovar[15–19], Davidson and Wood[15–19], and Kadzik et al.[15–19]). Indeed, in yeast, the Arp2/3 complex inhibition with drugs promotes formin-mediated cable formation, indicating a tension in the actin pool with implications for cell polarity.[20–24] Moreover, multiple studies across various organisms and model systems have shown that actin structures compete within cells, indicating a universal phenomenon where actin homeostasis prevents excessive network outgrowth, such as the Arp2/3 complex regulating formin activity during *C. elegans* embryo cytokinesis.[25] Furthermore, this competition is suggested to impact cell polarization and the initiation of motility[26–30] as well as the size regulation of structures like tunneling nanotubes and microvilli.[31–33]

Interestingly, in cells, multiple actin-based structures with various filament density and distinct nucleation rates can coexist despite their competition for actin monomers. For example lamellipodial networks, which rapidly consume actin monomers to elongate numerous filaments in dense arrays, do not prevent the growth of other networks, such as endocytic buds or cortical networks.[15,34,35] It seems that competition does not lead to binary outcomes, such as the survival or death of competitors. How these networks of varying strengths can coexist despite limited resources remains unknown. One possibility is that the pool of actin monomers is so large that the growth of each network does not restrict the others. However, the various examples above have shown that the growth of high- and low-consumption networks do depend on each other.[17] Another possibility is that the constant disassembly of actin-based structures replenishes the pool and tempers the competition. Indeed, most cellular actin architectures are renewed within minutes.[36,37] This turnover allows cells to respond to various perturbations or signaling events by dynamically adjusting the localization and size of their actin-based networks.[14,36,38] It might also participate in the coexistence of these networks in a competitive environment for resources. Whether and how actin-based structures turnover modulates their competition for resources and leads to complex outcomes, allowing their coexistence despite limited resources, remains an open question.

Theoretical studies have attempted to uncover mechanisms regulating the size of multiple structures from a finite set of components. Mohapatra et al.[39] found the limiting pool mechanism insufficient to explain the variation of their sizes. Interestingly, Suarez et al.[40] suggested that the various lifetimes of the structures are a key regulator of their competition. More recent works[41,42] proposed a theory involving negative feedback between growth rate and structure size. However, these theories lack experimental validation, and a comprehensive understanding of how dynamic actin networks share monomer pools remains elusive. Moreover, it is extremely challenging to precisely control the number, position, size, and nucleation rates of all actin-based structures in cells. This is why, in this study, we used a reconstituted system to investigate the parameters that enable the coexistence of actin networks in a controlled environment with limited resources. We used the actin-based motility assay to reconstitute branched actin networks (without or with turnover, as described in Colin et al.[43]) in microwells to limit the enclosed volume and the total amount of resources. Thereby, we reported the first reconstitution of the competition between dynamic architectures, in the presence of a limited pool of components. We show that the turnover of actin architectures ensures the redistribution of resources among them and thus allows the coexistence of networks of different strengths. Finally, we have highlighted the limits of this balancing system when faced with a large number of competing networks, leading to greater competition.

RESULTS

Without turnover, the size of the actin structures is determined by the pool of available monomers

To study the competition for actin monomers between multiple networks, we used the well-described bead motility assay.[43–51] Briefly, we coated 4.5-μm-diameter polystyrene beads with a nucleation-promoting factor (NPF, Snap-streptavidin-WA-His, see STAR Methods), triggering actin assembly via the Arp2/3 complex. We introduced these beads in cell-sized microwells (previously described in Colin et al.[43] and Yamamoto et al.[52]). The use of these microwells ensures control and limitation of the quantity of proteins present for the growth of actin structures.[53] We first grew actin comet tails in the presence of actin, profilin, capping protein, and the Arp2/3 complex (see STAR Methods for concentrations; Figure 1A). In these conditions, the turnover rate of the comet is extremely slow (less than 0.02 h^{-1}, Colin et al.[43]) so we consider this condition as "without turnover." We imaged the microwells containing the beads with fluorescence microscopy, and we analyzed the actin comet size as a function of the number of beads in the microwells (Figure 1B; Video S1). We calculated the structure size based on the measurement of comet area (STAR Methods). By measuring comet area per bead as a function of time (Figure 1C), we estimated that the growth of comets is completed in about 150 min. We therefore decided to measure the area of each individual comet at the growth plateau (also called steady state or stalled state), between 200 and 260 min. When the number of beads in the microwell increases, the size of each individual comet tail decreases, inversely proportional to the number of beads (Figure 1D). The estimate of actin polymerized within comet tails (STAR Methods) showed that the quantity of actin polymerized is approximately constant regardless of the number of beads in the microwell (Figure 1E). This can also be assessed by quantifying the amount of actin (monomers and oligomers, Colin et al.[43]) present in the microwell bulk at steady state, which remains constant regardless of the number of beads in the microwell (Figure S1A; STAR Methods). Mean density of comet tails slightly decreases when the number of beads in the microwell increases (Figure S1B), suggesting that there probably is a competition between nucleation and assembly when multiple structures grow simultaneously. We then estimated the amount of protein in the microwells (STAR Methods; Figure S1C) and concluded that neither the Arp2/3 complex nor the capping protein acts as a significant limiting factor. From these data, we conclude that without turnover, the size of actin structures depends on the number of competing structures. This size variation and the dependency on the inverse of the number of the beads can be attributed to a well-described mechanism involving a limited pool of resources,[54,55] where the actin pool is constrained and distributed equally among the various architectures (Figure 1F).

With turnover, the actin monomer pool is partially limited depending on turnover rate and is equally shared between competing structures

Next, we grew comet tails in microwells with slow or rapid actin turnover, incorporating disassembly (ADF/cofilin) and recycling (cyclase-associated protein, CAP) proteins at different concentrations (Figure 2A), to observe their effect on the size of competitive actin networks. With rapid turnover, the beads move at an average speed of 3 $\mu m/min^{-1}$, and the comets have an average length of 10 μm, corresponding to a turnover rate of approximately 0.3 min^{-1}. In other words, the comet is renewed every 3.3 min, which is similar to the turnover rate observed for the lamellipodia in cells.[56–58] We considered microwells containing

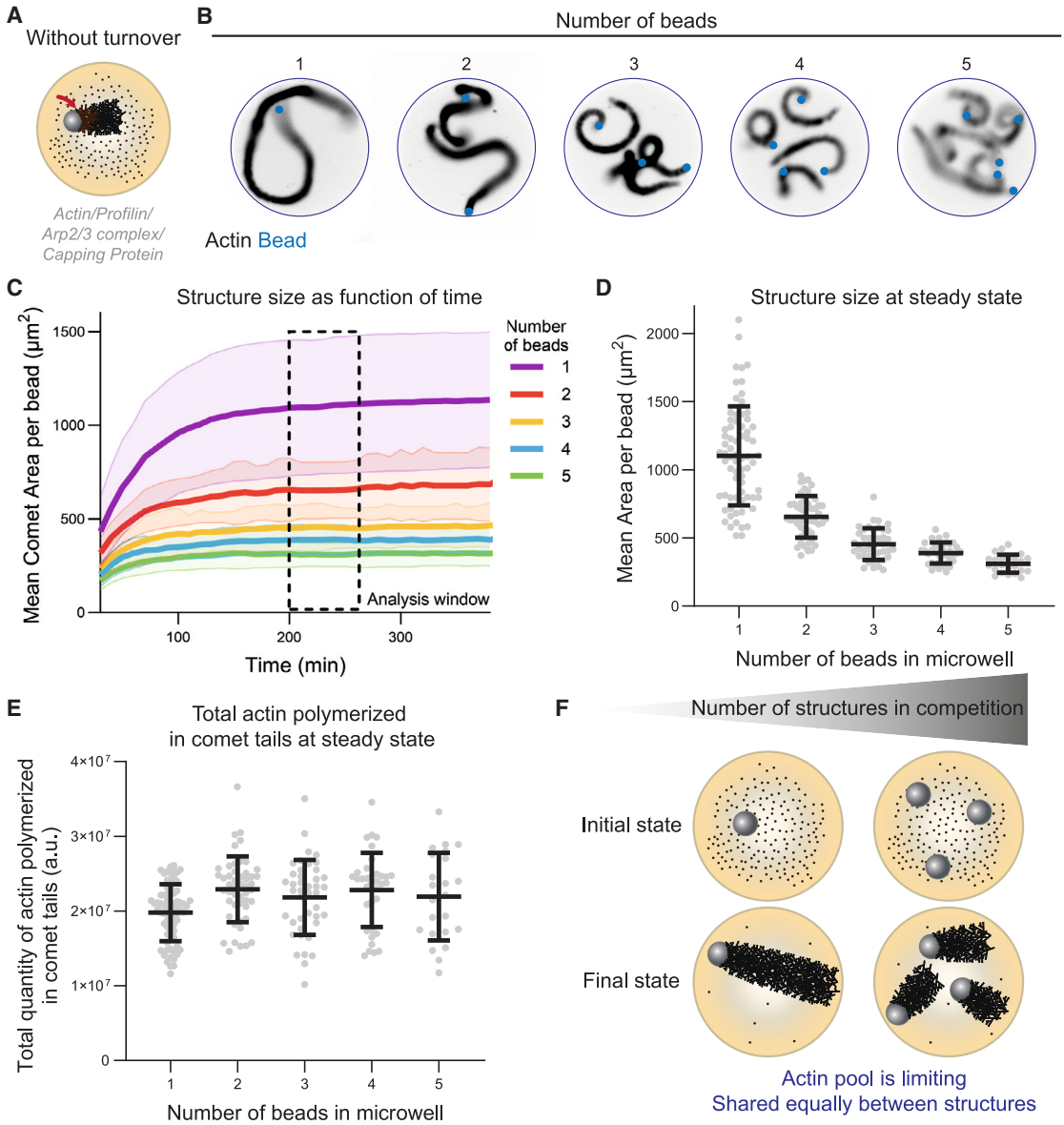

Figure 1. Without turnover, the size of the actin structures is determined by the pool of available monomers

(A) Scheme of the experimental setup (arrow shows the site of actin network assembly).

(B) Snapshots of actin comets (black) grown from polystyrene beads (blue) coated with a nucleation-promoting factor (NPF) of the Arp2/3 complex in microwells. Snapshots were taken after 6 h.

(C) Mean comet area per bead as a function of time for various numbers of beads in the microwell. Mean and standard deviation are represented.

(D) Mean comet area (structure size) per bead at steady state (between 3 and 4 h) as a function of the number of beads in the microwell. Gray circles represent individual microwells on top of which mean and standard deviation of the whole population are plotted. Dashed line represents a fit (area = A + B/number of beads, fit results: A = 136.2, B = 976.3, R^2 = 0.996).

(E) Total actin quantity in comet tails in steady state as a function of the number of beads in the microwell. Gray circles represent individual microwells on top of which mean and standard deviation of the whole population are plotted.

(F) Interpretation scheme: without turnover, the network size is determined by the available pool of proteins. *Replicates*: 4 independent experiments. 1 bead: $n = 70$ microwells, 2 beads = $n = 49$ microwells, 3 beads: $n = 42$ microwells, 4 beads: $n = 36$ microwells, 5 beads: $n = 23$ microwells. *Biochemical conditions*: 4.5 µm beads coated with 400 nM of SNAP-Strep-WA-His. Reaction mix: [actin] = 6 µM, [profilin] = 12 µM, [Arp2/3 complex] = 90 nM, [capping protein] = 40 nM.
See also Figure S1 and Video S1.

a varying number of beads (Figure 2B; Video S1). By monitoring the size of actin comets as a function of time (Figure 2C), we found that steady state is established after 50 min and is stable for over 300 min (as previously described in Colin et al.[43]). We quantified the comet area at steady state (between 120 and 180 min, Figure 2D). Remarkably, under conditions of rapid

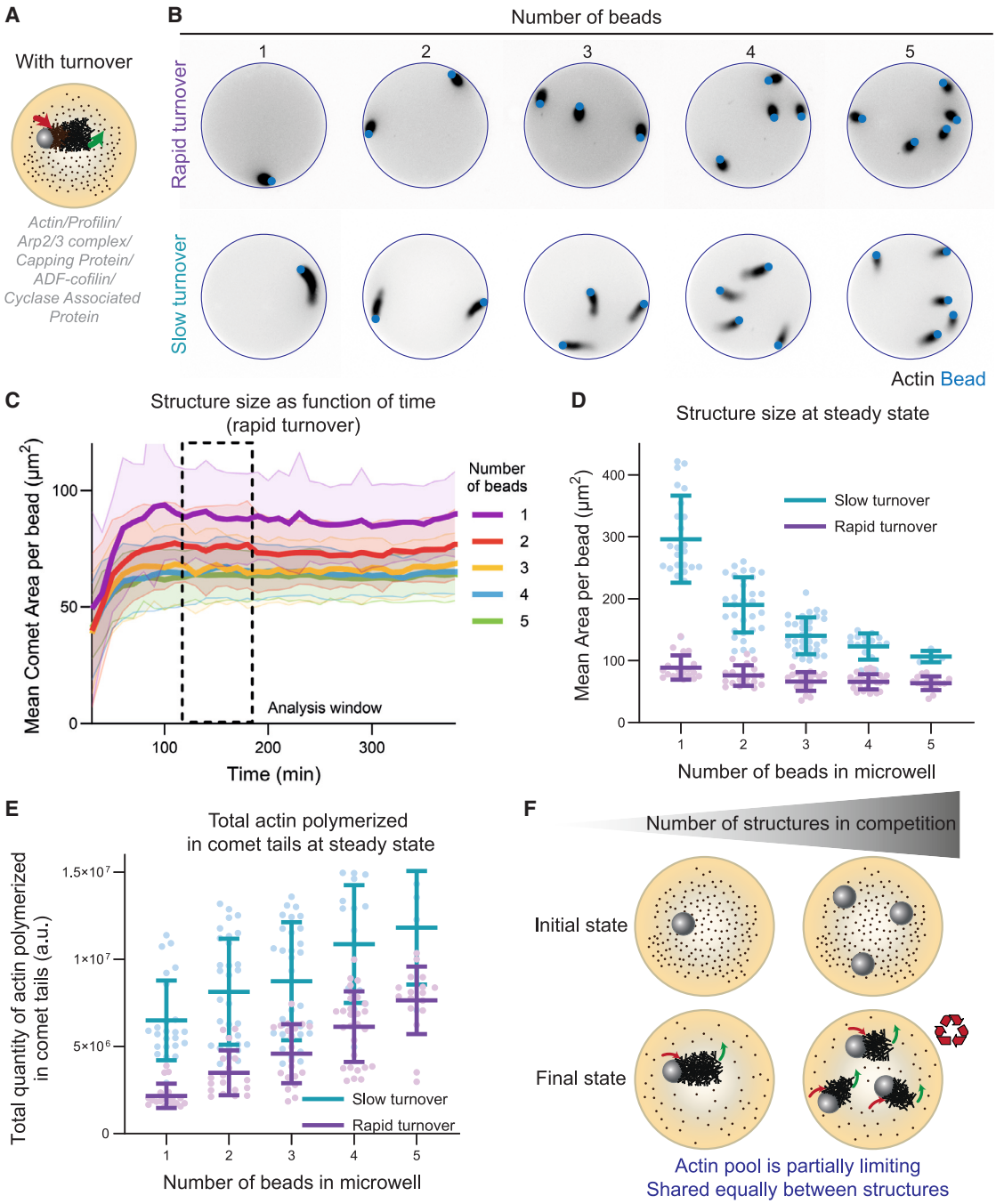

Figure 2. Depending on the turnover rate, the actin pool is no longer limiting

(A) Scheme of the experimental setup. Red and green arrows indicate assembly/disassembly, respectively.

(B) Snapshots of actin comets (black) grown from polystyrene beads (blue) coated with a nucleation-promoting factor (NPF) of the Arp2/3 complex in microwells with a high or low disassembly rate (see below for biochemical conditions). Snapshots were taken after 90 min.

(C) Mean comet area per bead as a function of time for various numbers of beads in the microwell (high disassembly conditions). Mean and standard deviation are represented.

(D) Mean comet area per bead at steady state (between 2 and 3 h) as a function of the number of beads in the microwell for low (blue) and high (pink) disassembly rates. Circles represent individual microwells on top of which mean and standard deviation of the whole population are plotted.

(E) Total actin quantity in comet tails at steady state as a function of the number of beads in the microwell for low (blue) and high (pink) disassembly rates. Circles represent individual microwells on top of which mean and standard deviation of the whole population are plotted.

(legend continued on next page)

turnover, the size of the comet tails becomes nearly independent of the number of beads in the microwells. Consequently, the total amount of actin polymerized in the comet tails increases with the number of beads in the microwell (Figure 2E), whereas it remains constant in conditions without turnover (Figure 1E). This demonstrates that rapid turnover dictates the size of the actin comet tails and constrains competition among different actin networks due to the high concentration of actin available in the microwell bulk (Figures 2F and S1D). Interestingly, in slow turnover conditions, we observed that the size of individual comet tails depends on the number of beads in the microwell (Figure 2D, blue curve), as observed in conditions without turnover (Figure 1D). The total amount of actin polymerized in the comet tails still increases with the number of beads in the microwell under these conditions (Figure 2E), demonstrating that the actin pool is only partially limited, as can also be seen from the quantification of actin available in the microwell bulk (Figure S1D). Based on these results, we investigated how limited or rapid turnover might influence the coexistence of branched networks with differing densities.

Without turnover, weak actin networks cannot coexist with strong networks when they are in competition

We prepared two types of beads with different concentrations of NPF (200 and 400 nM, referred to as low- and high-NPF densities, colored orange and blue, respectively, in Figures 3, 4, and 5). The low-density beads have a surface density of 3.8 NPF per 100 nm^2, while the high-density beads have a surface density of 7.6 NPF per 100 nm^2 (similar to the range reported in Wiesner et al.[59]). When grown in bulk (unlimited resources), the low- and high-NPF-density beads generated networks with sparse and dense densities, respectively (Figure S2A). The growth of comet tails with low-NPF density was initiated more slowly[59–61] (Figure S2B), and they incorporated actin at a slower rate, as evidenced by a linear fit of the actin quantity in the comet tail as a function of time (Figure S2B). Overall, given these properties of density and actin consumption rate, we define those networks as weak and strong, respectively. We then placed the low- and high-NPF-density beads in microwells. Without competition, both weak and strong actin tails were able to grow (Figure 3A, left; Video S2) and reached similar maximum sizes (Figure 3B, left). We then looked at the cases where the two networks (weak and strong) were in competition in the same microwell (Figure 3A, right; Video S2). Without turnover, the strong network maintained a similar size to that observed without competition. However, in all cases we tested, the weak network was unable to grow (Figures 3A and 3B, right; Video S2). This results in a size decrease of 100% for the weak network, whereas the size of the strong network decreases by only 3% (Figure 3E, left). Interestingly, regardless of the number of low-NPF-density beads in the microwell, their growth cannot initiate, whereas the high-NPF-density beads always initiate growth (Figures S2E and S2F). To understand why the weak network cannot initiate growth in the presence of competition, we first examined the kinetics of comet growth in the absence of competition. From the plots depicting the comet area over time (Figure S2C), it is evident that there is an approximately 40-min delay for the weak network (orange curve) to initiate its growth, compared with the strong network. If we analyze the actin available in the microwell bulk (STAR Methods), we observe that by the time the weak network begins to grow (at 40 min, Figure S2D), the strong network has already consumed 35% of the available actin. This indicates that the weak network encounters a concentration of only ~3.9 μM of actin, which is insufficient for efficient initiation of growth, as observed from the growth of comet tails in the flow chamber (Figures S2G and S2H).

Since the delay for actin comet growth depends on the initial symmetry-breaking step around the beads, we decided to test if this observation holds in a different geometry where there is no need for symmetry breaking in actin network growth. To do this, we used lipid micropatterns that closely mimic actin polymerization near a membrane, similar to conditions found in cells. We reported the lipid-patterning method recently,[62] and we adapted it here in microwells (see STAR Methods; Figure S3A). We passivated the microwells with silanePEG and then used the Primo device[63,64] to pattern the selected regions. Following this, we introduced biotin-functionalized lipids and streptavidin-functionalized NPF. Interestingly, using the Primo device, we can adjust the grayscale intensity of the input pattern to vary the degree of PEG layer removal. This results in different amounts of lipids (and consequently NPF) on the micropatterns (Figure S3B). The various quantities of NPF further lead to various actin network densities (Figure S3C). We used the fluorescence of the lipids as a proxy for the amount of NPF on our micropatterns. We analyzed the correlation between lipid fluorescence intensity and actin polymerization on each pattern (Figure S3C). The correlation coefficient between these two quantities is 0.91, demonstrating that lipid fluorescence intensity serves as a reliable readout of NPF density on the micropatterns. We then analyzed and compared the lipid fluorescence intensity of micropatterns burned under conditions without and with competition (Figure S3D). We concluded that the amount of lipids (both high and low density) remains the same, regardless of the number of micropatterns in the microwell (i.e., in conditions without or with competition).

As we observed for the beads coated with a low density of NPF, there is a delay for the low-NPF-density micropatterns to start their growth, and this delay directly depends on the NPF density (Figures S3E and S3F). This delay is probably due to the initial time for pattern seeding (primer effect, as described in Achard et al.[65]). In addition, we evaluated the actin consumption rate of networks grown from various NPF densities (Figure S3G), and we observed that high-NPF-density

(F) Interpretation scheme: depending on turnover rate, actin pool is no longer limiting and is shared equally between the structures. *Replicates*: low disassembly rate: 2 independent experiments. 1 bead: $n = 19$ microwells, 2 beads: $n = 19$ microwells, 3 beads: $n = 20$ microwells, 4 beads: $n = 28$ microwells, 5 beads: $n = 17$ microwells. High disassembly rate: 2 independent experiments. 1 bead: $n = 24$ microwells, 2 beads: $n = 31$ microwells, 3 beads: $n = 34$ microwells, 4 beads: $n = 17$ microwells, 5 beads: $n = 4$ microwells. *Biochemical conditions*: 4.5 μm beads coated with 400 nM of SNAP-Strep-WA-His. Reaction mix: [actin] = 6 μM, [profilin] = 12 μM, [Arp2/3 complex] = 90 nM, [capping protein] = 40 nM. High disassembly rate: [ADF/cofilin] = 800 nM, [CAP] = 400 nM. Low disassembly rate: [ADF/cofilin] = 400 nM, [CAP] = 200 nM.
See also Figure S1 and Video S1.

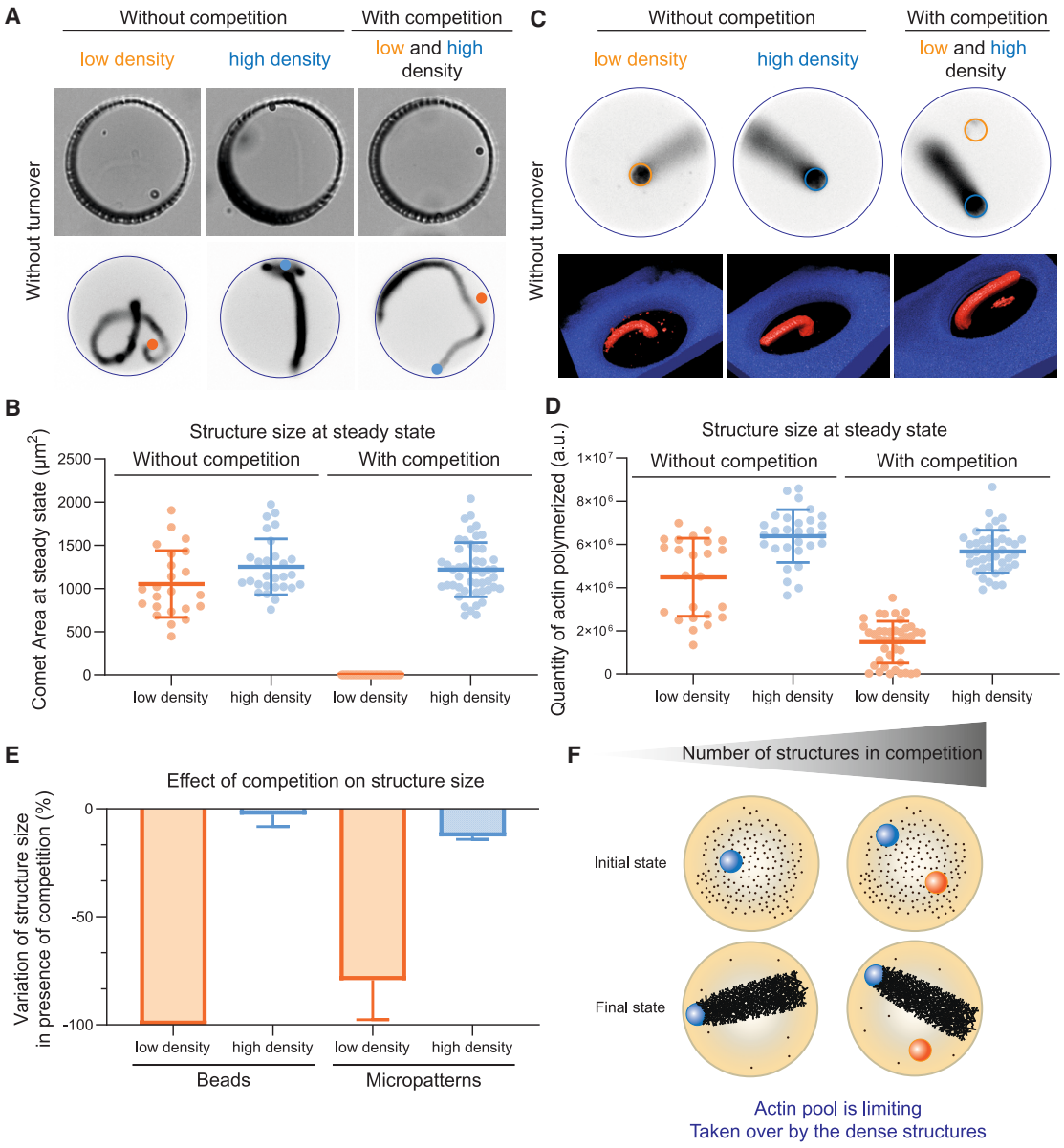

Figure 3. When structures with various densities compete without turnover, the actin monomer pool is consumed preferentially by denser structures

(A) Snapshots (top row: bright field, bottom row: fluorescence with actin in black) of actin comet tails grown from polystyrene beads coated with a nucleation-promoting factor (NPF, blue bead: high-NPF density – 400 nM WA, orange bead: low-NPF density – 200 nM WA) of the Arp2/3 complex in microwells in conditions without turnover. Snapshots were taken after 300 min.

(B) Comet area at steady state for comets grown from low-NPF-density (orange) and high-NPF-density (blue) beads, in the absence or presence of competition. Colored circles represent individual microwells on top of which mean and standard deviation of the whole population are plotted.

(C) Snapshots (top row) and 3D reconstructions (bottom row) of actin branched networks grown from lipid micropatterns with various densities of NPF (orange: low and blue: high). For the 3D reconstructions: actin is shown in red.

(D) Quantity of actin polymerized at steady state for structures grown on low-density and high-density patterns, in the absence or presence of competition. Colored circles represent individual microwells on top of which mean and standard deviation of the whole population are plotted.

(E) Variation of structure size in the presence of competition expressed as a percentage. The mean variation of structure size is computed per independent dataset, and standard deviation represents the variation between independent datasets.

(F) Interpretation scheme: without turnover, when structures with various densities are in competition, the actin monomer pool is limiting and is taken over by the dense structures.

Replicates: beads: 3 independent experiments. Without competition, low-NPF density: $n = 23$ microwells. Without competition, high-NPF density: $n = 28$ microwells. With competition, $n = 49$ microwells.

(legend continued on next page)

networks are consuming actin monomers at a faster rate than low-NPF-density networks. Therefore, given those characteristics, we were able to generate weak and strong actin networks that grew in 3D in the microwell in conditions without and with competition (Figure 3C; Video S3). We observed that without turnover, similar to what was described with the beads in competitive scenarios, the weak network could barely grow, whereas it could grow when there was no competition. We confirmed this observation with the 3D reconstruction of the networks and with the quantification of actin polymerized on the different patterns (Figures 3C and 3D). In this competitive condition, the weak network size decreases by 79%, whereas the strong network size decreases only by 13% (Figure 3E). Thus, with another geometry (micropattern), we confirmed the results obtained with the beads. In the case of micropatterns, we can explain this result by the delay in the initiation of growth and the varying actin consumption rates of networks with different densities. Specifically, we observed that high-NPF-density networks initiate growth quicker and consume actin monomers faster than low-NPF-density networks (Figures S3F and S3G). Therefore, in the presence of competition, the available pool of monomers in the microwell is depleted very rapidly due to the strong network (Figure S3H), limiting the amount of actin available in the microwell bulk when the weaker network begins to grow. Overall, we show that depending on the time they take to initiate growth and their rate of monomer consumption, actin networks grown from patterns with varying NPF densities are affected to different extents by competition (Figure S3I).

We conclude that in the absence of turnover, the actin monomer pool acts as a limiting factor for competitive networks to coexist. When architectures of different densities compete with one another, the denser networks dominate the available resources in a "winner-takes-all" process, thereby preventing the weak networks from growing (Figure 3F). We next sought to evaluate whether under conditions with rapid turnover, the system operates differently according to the possible coexistence of networks with different strengths.

Rapid turnover ensures a balanced distribution of resources, thereby enabling the existence of networks of different strengths

We then tested conditions with rapid turnover (addition of ADF/cofilin and CAP to the experiment) for beads and micropatterns geometries. For the bead geometry without competition, both weak and strong networks were growing, with strong comets being a bit longer than weak ones (Figures 4A and 4B; Video S4). When the two networks were in competition in the same microwell, we observed that they were both growing and coexisting over a long period of time. The size of the strong network was unaffected by the competition (Figure 4E), and the size of the weak network was moderately affected by the competition (decrease of 65%, Figure 4E). This shows that rapid turnover enables the existence of weak networks that could not grow without it. Indeed, in the presence of turnover, there is a sizable pool of monomers that is shared because of rapid monomer diffusion. We estimated that in conditions with competition, there is 5 μM of actin available in the microwell bulk (Figure S4A). Therefore, some monomers always reach the weak bead surface and can assemble into the tail of the network at that location.

We next examined the same configuration with rapid turnover of actin networks grown from micropatterns. Similar to our observations with the beads, we found that in the presence of turnover, both weak and strong networks could grow and coexist (Figures 4C and 4D; Video S5). Therefore, we conclude that rapid turnover allows the protein pool to be distributed, accommodating varying strengths of these networks as they grow (Figure 4F). However, under competitive conditions, both weak and strong networks showed a 20% reduction in size, which can be explained by the fact that with micropatterns, there is less actin available in the microwell bulk, compared with the bead situation (Figures S4A and S4B). This result suggests limitations in balancing resources among different actin networks (Figure 4E). We therefore aimed to challenge the limits of the rapid turnover condition concerning resource balance between structures with varying strengths.

When numerous structures compete, the actin monomer pool becomes limiting again, leading to the disappearance of the sparse network population

To do this, we examined scenarios where many beads were present in the microwells. We counted the number of high-NPF-density beads (in blue on the figure) in the microwell and defined this number as representative of the strength of competition (Figure 5A; Video S6). We then examined the percentage of low-NPF-density beads (orange on the figure) that initiate growth, as a function of competition strength (Figure 5B). We observed that when the level of competition is low (less than two high-density beads), most low-density beads could grow a comet. Then, in the medium range of competition, we observed a selection process, meaning that only a fraction of low-density beads could grow a comet and move. Interestingly, when we computed the actin available in the microwell bulk in these experiments (Figure S4C), we observed that above two strong beads, there is a plateau in the amount of actin available, corresponding to the point at which the selection process begins. Therefore, with more than two strong beads, the actin pool becomes limited, and the system selectively favors structures that can grow, preventing some of the weaker structures from doing so. When the level of competition is high (more than six high-density beads), weak networks cannot grow (Figure 5C). Interestingly, when high-NPF-density beads are alone in the microwell (conditions of Figure 2), they reach a plateau for the total actin polymerized in comet tails at steady state after six beads

Micropatterns: 2 independent experiments. Without competition, low-NPF density: $n = 24$ microwells. Without competition, high-NPF density: $n = 29$ microwells. With competition, $n = 42$ microwells.

Biochemical conditions: 4.5 μm beads coated with 400 or 200 nM of SNAP-Strep-WA-His. Reaction mix for assembly conditions: [actin] = 6 μM, [profilin] = 12 μM, [Arp2/3 complex] = 90 nM, [capping protein] = 40 nM.

Micropatterns: lipids with 0.5% of biotin; coating with 50 nM of SNAP-Strep-WA-His. Same reaction mix as for the beads.

See also Figures S2 and S3 and Videos S2 and S3.

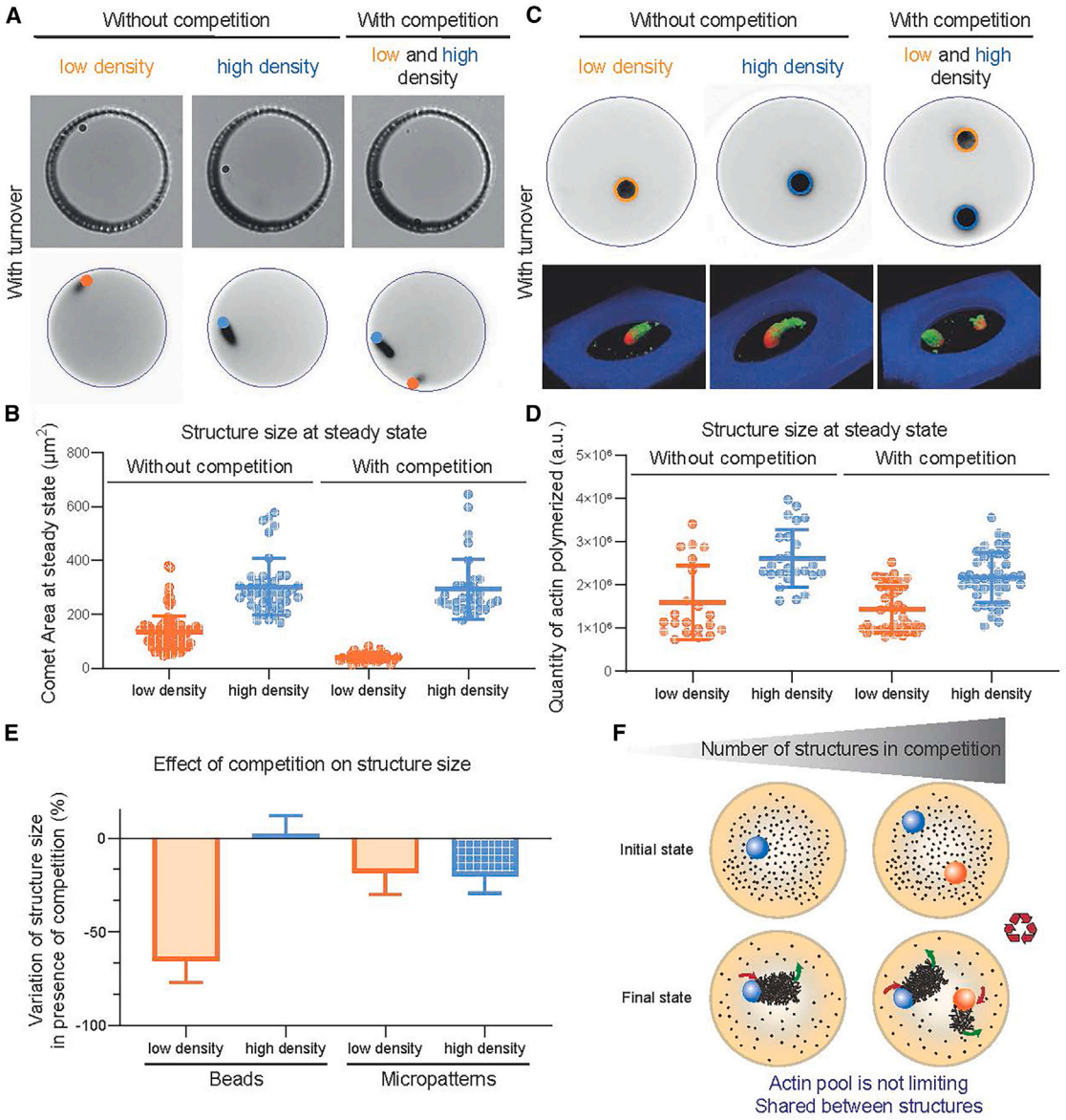

Figure 4. Conditions with turnover allow the coexistence of actin networks with various densities

(A) Snapshots (top row: bright field, bottom row: fluorescence with actin in black) of actin comet tails grown from polystyrene beads coated with a nucleation-promoting factor (NPF, blue bead: high-NPF density – 400 nM WA, orange bead: low-NPF density – 200 nM WA) of the Arp2/3 complex in microwells in conditions with turnover. Snapshots were taken after 240 min.

(B) Comet area at steady state for comets grown from low-density (orange) and high-density (blue) beads, in the absence or presence of competition. Colored circles represent individual microwells on top of which mean and standard deviation of the whole population are plotted.

(C) Snapshots (top row) and 3D reconstructions (bottom row) of actin branched networks grown from lipid micropatterns with various densities of NPF (orange: weak and blue: strong) in conditions with turnover. For the 3D reconstructions: actin is shown in red and fluorescently labeled ADF/cofilin is shown in green.

(D) Quantity of actin polymerized at steady state for structures grown on low-density and high-density patterns, in the absence or presence of competition in conditions with turnover. Colored circles represent individual microwells on top of which mean and standard deviation of the whole population are plotted.

(E) Variation of structure size in the presence of competition expressed as a percentage. The mean variation of structure size is computed per independent dataset, and standard deviation represents the variation between independent datasets.

(F) Interpretation scheme: protein turnover is necessary to limit the competition and to allow the coexistence of structures with various densities. *Replicates:* beads: 3 independent experiments. Without competition, low-NPF density: n = 94 microwells. Without competition, high-NPF density: n = 41 microwells. With competition, n = 32 microwells.

(legend continued on next page)

in the microwell (Figure S4D). We therefore conclude that beyond a certain number of structures, rapid turnover alone cannot ensure the coexistence of all networks. The actin pool becomes limiting once again, and the strongest networks are the ones that ultimately "win it all."

DISCUSSION

Our findings highlight the necessity of considering protein turnover to understand the mechanisms that allow the coexistence of various structures competing for a limited pool of components.

Under conditions without turnover, the outcome is dictated by the mere consumption rates of resources, and the system is rapidly trapped in its final configuration, preventing further evolution. Weak structures cannot develop, and only strong structures dominate the final architecture. The result is not only homogeneous but also static. Indeed, while this leads to high stability, it lacks adaptive properties. In cells, some structures like stereocilia or sarcomeres have an extremely low turnover (from hours to days[66,67]). However, both types of structures continue to incorporate actin at their tips, which is necessary for their maintenance through the organism's life[68–71]). An intriguing question is, what prevents protein degradation or possible damage in these long-lived structures, as observed in reconstituted systems?[43] The potential existence of a repair mechanism that maintains cytoskeletal integrity after damage is an exciting possibility.[72,73]

Under turnover conditions, structures first consume resources as they establish a steady state. Then resources are recycled, and at steady state, the net consumption of resources is effectively zero, and the size remains constant. Interestingly, the slow turnover condition represents an intermediate scenario where the slower recycling of resources limits their availability, thereby affecting the size of the structures. Our results also show that competition for resources intensifies when structures with varying strengths coexist. Without turnover, structures deplete resources quickly, leaving little for weaker structures to grow. However, turnover mitigates this issue up to a certain extent. In cells, branched networks involved in key functions like motility and endocytosis compete for actin monomers,[74,75] and within structures like lamellipodia, density variations affect function and movement direction.[76–79] This study suggests that rapid turnover allows the redistribution of resources and the maintenance of weak structures generated by poor nucleation. Thus, the rapid renewal of dynamic structures such as lamellipodia could allow the coexistence of networks with large variations of densities.[34,35] Generally speaking, at all levels of life, turnover is an essential monitoring system and is indispensable for the reuse of components.[80] However, turnover is costly in energy, and there is therefore a trade-off between the turnover, the adaptability of the system when facing a perturbation, and the energy cost. Reduction or modulation of turnover rate can then be a strategy to reduce the energy consumption, during hibernation[81] or quiescent phases,[82] for example.

By examining the system's limits, we have demonstrated that even under fast turnover, excessive competition can force the system to select which structures can polymerize and persist. This decision-making process, which influences the formation or loss of structures, may additionally involve activating signaling pathways or reallocating resources based on turnover rates.[12,83,84] For instance, cytochalasin-D treatment typically eliminates fast-turnover structures, such as lamellipodia, while low-turnover structures, like stress fibers, remain unaffected.[85] This phenomenon may be attributed to the competition strength caused by cytochalasin-D, which disrupts the coexistence of structures. This work does not address the competition between different actin architectures, such as branched versus linear networks, nor does it address how cellular compartmentalization and heterogeneity might influence this competition.[19] Future studies should explore these aspects, including the impact of local actin monomer synthesis[86] on the distribution among competing actin networks.

Our study emphasizes the crucial role of competition strength, shaped by turnover rate, protein pool size, and the number of competing structures. These factors interact through feedback mechanisms, with high turnover reducing competition and lower turnover increasing protein consumption, therefore affecting the coexistence of actin architectures. Modulating competition strength, by varying the amount of available monomers, significantly affects actin structure size and shape, impacting cellular functions like polarization and migration.[26,87–89] Additionally, a larger pool of monomers may reduce the competition strength, as evidenced by the increased number of stress fibers in larger cells.[90,91] Interestingly, contrary to the notion that "bigger is better," evolution appears to favor finite reservoirs, which leads to higher fitness and consistency.[6] Indeed, a limited protein pool and a high competition strength enable structures to assess one another's activity based on resource availability, with protein concentration influencing turnover rates and assembly.[5,6,54,92]

RESOURCE AVAILABILITY

Lead contact

Further information and requests for resources and reagents should be directed to and will be fulfilled by the lead contact, Alexandra Colin (alexandra.colin@cnrs.fr).

Materials availability

- This study did not generate new unique reagents.

Data and code availability

- All raw imaging data are freely available and will be shared by the lead contact upon request.

Micropatterns: 2 independent experiments. Without competition, low-NPF density: $n = 21$ microwells. Without competition, high-NPF density: $n = 25$ microwells. With competition, $n = 42$ microwells. *Biochemical conditions:* 4.5 μm beads coated with 400 or 200 nM of SNAP-Strep-WA-His. [Actin] = 6 μM, [profilin] = 12 μM, [Arp2/3 complex] = 90 nM, [capping protein] = 40 nM, [ADF/cofilin] = 800 nM, [CAP] = 400 nM.
Micropatterns: lipids with 0.5% of biotin; coating with 50 nM of SNAP-Strep-WA-His. [Actin] = 6 μM, [profilin] = 12 μM, [Arp2/3 complex] = 90 nM, [capping protein] = 40 nM, [ADF/cofilin] = 400 nM, [CAP] = 200 nM.
See also Figure S4 and Videos S4 and S5.

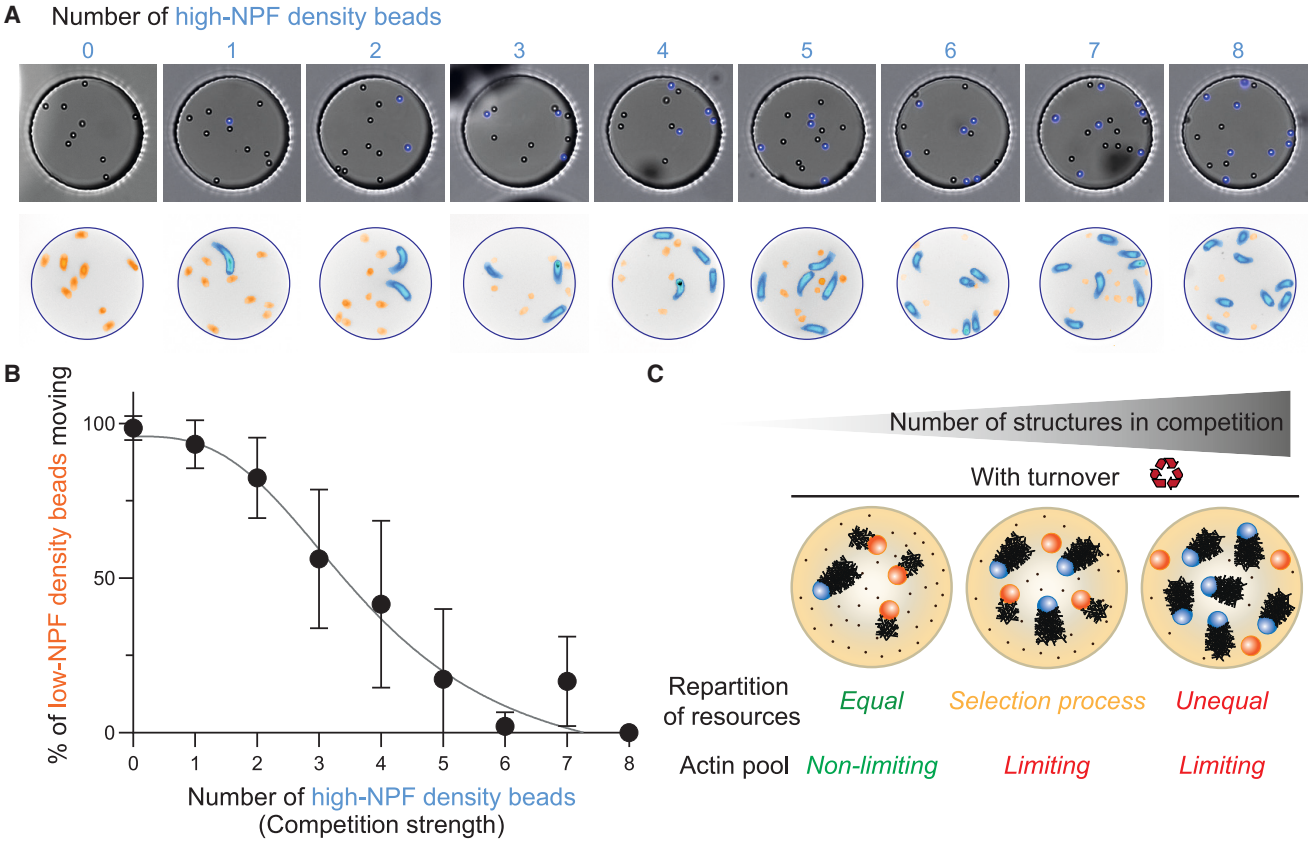

Figure 5. When too many structures are in competition, the actin monomer pool becomes limiting again

(A) Snapshots of microwells with various numbers of high-NPF-density beads (blue beads).

(B) Quantification of the percentage of low-NPF-density beads moving (orange beads), as a function of the number of high-NPF-density beads (blue beads) in the microwell. Mean and standard deviation of the whole population are plotted.

(C) Interpretation scheme. With turnover, the repartition of resources is equal, and the monomer pool is not limiting until a certain number of structures are reached. *Biochemical conditions*: 4.5 μm beads coated with 400 or 200 nM of SNAP-Strep-WA-His. [Actin] = 6 μM, [profilin] = 12 μM, [Arp2/3 complex] = 90 nM, [capping protein] = 40 nM, [ADF/cofilin] = 800 nM, [CAP] = 400 nM. *Replicates*: 2 independent experiments. 0 high-NPF-density beads: n = 8 microwells, 1 high-NPF-density bead: n = 16 microwells, 2 high-NPF-density beads: n = 29 microwells, 3 high-NPF-density beads: n = 23 microwells, 4 high-NPF-density beads: n = 20 microwells, 5 high-NPF-density beads: n = 8 microwells, 6 high-NPF-density beads: n = 11 microwells, 7 high-NPF-density beads: n = 3 microwells, 8 high-NPF-density beads: n = 1 microwell.

See also Figure S4 and Video S6.

- This paper does not report original code.
- Any additional information required to reanalyze the data reported in this paper is available from the lead contact upon request.

ACKNOWLEDGMENTS

We thank Benoit Vianay for insightful discussions. This work was supported by the European Research Council (consolidator grant 771599 [ICEBERG] to M.T. and advanced grant 741773 [AAA] to L.B.), the grant ANR-23-CE13-0023-MOVING to L.B. and the grant ANR-24-CE13-3582 SCALING to A.C. This work was also supported by the MuLife imaging facility, which is funded by GRAL, a program from the Chemistry Biology Health Graduate School of University Grenoble Alpes (ANR-17-EURE-0003). A.C. thanks CNRS Biology for the allocation of new CNRS entrants.

AUTHOR CONTRIBUTIONS

Conceptualization, A.C., L.B., C.G., M.T., and A.M.; investigation, C.G., A.C., A.-B.N., and L.G.; methodology, C.G. and A.C.; data curation, A.C.; project administration, A.C., L.B., and M.T.; funding acquisition, A.C., L.B., and M.T.; writing – original draft, A.C. and L.B.; writing – review and editing, A.C., L.B., M.T., and A.M.

DECLARATION OF INTERESTS

The authors declare no competing interests.

STAR★METHODS

Detailed methods are provided in the online version of this paper and include the following:

- KEY RESOURCES TABLE
- EXPERIMENTAL MODEL AND STUDY PARTICIPANT DETAILS
  - Protein purification
  - Polystyrene beads coating
  - Estimation of protein density on beads
  - Microwells preparation
  - Lipids/SUV preparation

- SilanePEG30k slides
- Bead motility assay in microwells
- Micropatterning in microwells
- Imaging

- QUANTIFICATION AND STATISTICAL ANALYSIS
  - Image analysis
  - Characterization of structure size for beads experiments
  - Characterization of structure size for micropatterns experiments
  - Estimation of the ratio of actin consumed from bulk in the comet tail
  - Estimation of protein quantity in microwells and of their consumption in experiments

SUPPLEMENTAL INFORMATION

Supplemental information can be found online at https://doi.org/10.1016/j.cub.2024.11.067.

Received: September 18, 2024
Revised: November 5, 2024
Accepted: November 26, 2024
Published: January 9, 2025

REFERENCES

1. Lotka, A.J. (1978). The growth of mixed populations: two species competing for a common food supply. J. Wash. Acad. Sci. *22*, 461–469. https://doi.org/10.1007/978-3-642-50151-7_12.
2. May, R.M. (1971). Stability in multispecies community models. Math. Biosci. *12*, 59–79. https://doi.org/10.1016/0025-5564(71)90074-5.
3. Lankau, R.A. (2011). Rapid evolutionary change and the coexistence of species. Annu. Rev. Ecol. Evol. Syst. *42*, 335–354. https://doi.org/10.1146/annurev-ecolsys-102710-145100.
4. Chesson, P. (2000). Mechanisms of maintenance of species diversity. Annu. Rev. Ecol. Syst. *31*, 343–366. https://doi.org/10.1146/annurev.ecolsys.31.1.343.
5. Gawne, R., McKenna, K.Z., and Levin, M. (2020). Competitive and coordinative interactions between body parts produce adaptive developmental outcomes. BioEssays *42*, e1900245. https://doi.org/10.1002/bies.201900245.
6. Smiley, P., and Levin, M. (2022). Competition for finite resources as coordination mechanism for morphogenesis: an evolutionary algorithm study of digital embryogeny. Biosystems. *221*, 104762. https://doi.org/10.1016/j.biosystems.2022.104762.
7. Díaz, B., and Moreno, E. (2005). The competitive nature of cells. Exp. Cell Res. *306*, 317–322. https://doi.org/10.1016/j.yexcr.2005.03.017.
8. Merino, M.M., Levayer, R., and Moreno, E. (2016). Survival of the fittest: essential roles of cell competition in development, aging, and cancer. Trends Cell Biol. *26*, 776–788. https://doi.org/10.1016/j.tcb.2016.05.009.
9. Clavería, C., and Torres, M. (2016). Cell competition: mechanisms and physiological roles. Annu. Rev. Cell Dev. Biol. *32*, 411–439. https://doi.org/10.1146/annurev-cellbio-111315-125142.
10. Taylor, T.B., Wass, A.V., Johnson, L.J., and Dash, P. (2017). Resource competition promotes tumour expansion in experimentally evolved cancer. BMC Evol. Biol. *17*, 268. https://doi.org/10.1186/s12862-017-1117-6.
11. Moreno, E. (2008). Is cell competition relevant to cancer? Nat. Rev. Cancer *8*, 141–147. https://doi.org/10.1038/nrc2252.
12. Baghdassarian, H.M., and Lewis, N.E. (2024). Resource allocation in mammalian systems. Biotechnol. Adv. *71*, 108305. https://doi.org/10.1016/j.biotechadv.2023.108305.
13. Blanchoin, L., Boujemaa-Paterski, R., Sykes, C., and Plastino, J. (2014). Actin dynamics, architecture, and mechanics in cell motility. Physiol. Rev. *94*, 235–263. https://doi.org/10.1152/physrev.00018.2013.
14. Lappalainen, P., Kotila, T., Jégou, A., and Romet-Lemonne, G. (2022). Biochemical and mechanical regulation of actin dynamics. Nat. Rev. Mol. Cell Biol. *23*, 836–852. https://doi.org/10.1038/s41580-022-00508-4.
15. Michelot, A., and Drubin, D.G. (2011). Building distinct actin filament networks in a common cytoplasm. Curr. Biol. *21*, R560–R569. https://doi.org/10.1016/j.cub.2011.06.019.
16. Rotty, J.D., and Bear, J.E. (2014). Competition and collaboration between different actin assembly pathways allows for homeostatic control of the actin cytoskeleton. BioArchitecture *5*, 27–34. https://doi.org/10.1080/19490992.2015.1090670.
17. Suarez, C., and Kovar, D.R. (2016). Internetwork competition for monomers governs actin cytoskeleton organization. Nat. Rev. Mol. Cell Biol. *17*, 799–810. https://doi.org/10.1038/nrm.2016.106.
18. Davidson, A.J., and Wood, W. (2016). Unravelling the actin cytoskeleton: A new competitive edge? Trends Cell Biol. *26*, 569–576. https://doi.org/10.1016/j.tcb.2016.04.001.
19. Kadzik, R.S., Homa, K.E., and Kovar, D.R. (2020). F-actin cytoskeleton network self-organization through competition and cooperation. Annu. Rev. Cell Dev. Biol. *36*, 35–60. https://doi.org/10.1146/annurev-cellbio-032320-094706.
20. Sagot, I., Klee, S.K., and Pellman, D. (2002). Yeast formins regulate cell polarity by controlling the assembly of actin cables. Nat. Cell Biol. *4*, 42–50. https://doi.org/10.1038/ncb719.
21. Gao, L., and Bretscher, A. (2008). Analysis of unregulated Formin activity reveals how yeast can balance F-actin assembly between different microfilament-based organizations. Mol. Biol. Cell *19*, 1474–1484. https://doi.org/10.1091/mbc.e07-05-0520.
22. Burke, T.A., Christensen, J.R., Barone, E., Suarez, C., Sirotkin, V., and Kovar, D.R. (2014). Homeostatic actin cytoskeleton networks are regulated by assembly factor competition for monomers. Curr. Biol. *24*, 579–585. https://doi.org/10.1016/j.cub.2014.01.072.
23. Suarez, C., Carroll, R.T., Burke, T.A., Christensen, J.R., Bestul, A.J., Sees, J.A., James, M.L., Sirotkin, V., and Kovar, D.R. (2015). Profilin regulates F-actin network homeostasis by favoring Formin over Arp2/3 complex. Dev. Cell *32*, 43–53. https://doi.org/10.1016/j.devcel.2014.10.027.
24. Billault-Chaumartin, I., and Martin, S.G. (2019). Capping protein insulates Arp2/3-assembled actin patches from formins. Curr. Biol. *29*, 3165–3176.e6. https://doi.org/10.1016/j.cub.2019.07.088.
25. Chan, F.-Y., Silva, A.M., Saramago, J., Pereira-Sousa, J., Brighton, H.E., Pereira, M., Oegema, K., Gassmann, R., and Carvalho, A.X. (2019). The Arp2/3 complex prevents excessive formin activity during cytokinesis. Mol. Biol. Cell *30*, 96–107. https://doi.org/10.1091/mbc.E18-07-0471.
26. Lomakin, A.J., Lee, K.-C., Han, S.J., Bui, D.A., Davidson, M., Mogilner, A., and Danuser, G. (2015). Competition for actin between two distinct F-actin networks defines a bistable switch for cell polarization. Nat. Cell Biol. *17*, 1435–1445. https://doi.org/10.1038/ncb3246.
27. Mejillano, M.R., Kojima, S., Applewhite, D.A., Gertler, F.B., Svitkina, T.M., and Borisy, G.G. (2004). Lamellipodial versus filopodial mode of the actin nanomachinery: pivotal role of the filament barbed end. Cell *118*, 363–373. https://doi.org/10.1016/j.cell.2004.07.019.
28. Dimchev, G., Steffen, A., Kage, F., Dimchev, V., Pernier, J., Carlier, M.-F., and Rottner, K. (2017). Efficiency of lamellipodia protrusion is determined by the extent of cytosolic actin assembly. Mol. Biol. Cell *28*, 1311–1325. https://doi.org/10.1091/mbc.E16-05-0334.
29. Dimchev, V., Lahmann, I., Koestler, S.A., Kage, F., Dimchev, G., Steffen, A., Stradal, T.E.B., Vauti, F., Arnold, H.-H., and Rottner, K. (2021). Induced Arp2/3 complex depletion increases FMNL2/3 Formin expression and filopodia formation. Front. Cell Dev. Biol. *9*, 634708. https://doi.org/10.3389/fcell.2021.634708.
30. Cao, L.G., Babcock, G.G., Rubenstein, P.A., and Wang, Y.L. (1992). Effects of profilin and profilactin on actin structure and function in living cells. J. Cell Biol. *117*, 1023–1029. https://doi.org/10.1083/jcb.117.5.1023.

31. Henderson, J.M., Ljubojevic, N., Belian, S., Chaze, T., Castaneda, D., Battistella, A., Giai Gianetto, Q., Matondo, M., Descroix, S., Bassereau, P., and Zurzolo, C. (2023). Tunnelling nanotube formation is driven by Eps8/IRSp53-dependent linear actin polymerization. EMBO J. *42*, e113761. https://doi.org/10.15252/embj.2023113761.

32. Faust, J.J., Millis, B.A., and Tyska, M.J. (2019). Profilin-mediated actin allocation regulates the growth of epithelial microvilli. Curr. Biol. *29*, 3457–3465.e3. https://doi.org/10.1016/j.cub.2019.08.051.

33. Chinowsky, C.R., Pinette, J.A., Meenderink, L.M., Lau, K.S., and Tyska, M.J. (2020). Nonmuscle myosin-2 contractility-dependent actin turnover limits the length of epithelial microvilli. Mol. Biol. Cell *31*, 2803–2815. https://doi.org/10.1091/mbc.E20-09-0582.

34. Chhabra, E.S., and Higgs, H.N. (2007). The many faces of actin: matching assembly factors with cellular structures. Nat. Cell Biol. *9*, 1110–1121. https://doi.org/10.1038/ncb1007-1110.

35. Campellone, K.G., Lebek, N.M., and King, V.L. (2023). Branching out in different directions: emerging cellular functions for the Arp2/3 complex and WASP-family actin nucleation factors. Eur. J. Cell Biol. *102*, 151301. https://doi.org/10.1016/j.ejcb.2023.151301.

36. Goode, B.L., Eskin, J., and Shekhar, S. (2023). Mechanisms of actin disassembly and turnover. J. Cell Biol. *222*, e202309021. https://doi.org/10.1083/jcb.202309021.

37. Théry, M., and Blanchoin, L. (2024). Reconstituting the dynamic steady states of actin networks in vitro. Nat. Cell Biol. *26*, 494–497. https://doi.org/10.1038/s41556-024-01379-x.

38. Plastino, J., and Blanchoin, L. (2018). Dynamic stability of the actin ecosystem. J. Cell Sci. *132*, jcs219832. https://doi.org/10.1242/jcs.219832.

39. Mohapatra, L., Lagny, T.J., Harbage, D., Jelenkovic, P.R., and Kondev, J. (2017). The limiting-pool mechanism fails to control the size of multiple organelles. Cell Syst. *4*, 559–567.e14. https://doi.org/10.1016/j.cels.2017.04.011.

40. Suarez, C., McCall, P.M., Gardel, M.L., and Kovar, D.R. (2017). When is "enough" enough? Cell Syst. *4*, 480–482. https://doi.org/10.1016/j.cels.2017.05.007.

41. Banerjee, D.S., and Banerjee, S. (2022). Size regulation of multiple organelles competing for a limiting subunit pool. PLoS Comput. Biol. *18*, e1010253. https://doi.org/10.1371/journal.pcbi.1010253.

42. Banerjee, D.S., and Banerjee, S. (2022). Emergence and maintenance of variable-length actin filaments in a limiting pool of building blocks. Biophys. J. *121*, 2436–2448. https://doi.org/10.1016/j.bpj.2022.05.014.

43. Colin, A., Kotila, T., Guérin, C., Orhant-Prioux, M., Vianay, B., Mogilner, A., Lappalainen, P., Théry, M., and Blanchoin, L. (2023). Recycling of the actin monomer pool limits the lifetime of network turnover. EMBO J. *42*, e112717. https://doi.org/10.15252/embj.2022112717.

44. Loisel, T.P., Boujemaa, R., Pantaloni, D., and Carlier, M.-F. (1999). Reconstitution of actin-based motility of Listeria and Shigella using pure proteins. Nature *401*, 613–616. https://doi.org/10.1038/44183.

45. Cameron, L.A., Footer, M.J., van Oudenaarden, A., and Theriot, J.A. (1999). Motility of ActA protein-coated microspheres driven by actin polymerization. Proc. Natl. Acad. Sci. USA *96*, 4908–4913. https://doi.org/10.1073/pnas.96.9.4908.

46. Bernheim-Groswasser, A., Wiesner, S., Golsteyn, R.M., Carlier, M.-F., and Sykes, C. (2002). The dynamics of actin-based motility depend on surface parameters. Nature *417*, 308–311. https://doi.org/10.1038/417308a.

47. Cameron, L.A., Robbins, J.R., Footer, M.J., and Theriot, J.A. (2004). Biophysical parameters influence actin-based movement, trajectory, and initiation in a cell-free system. Mol. Biol. Cell *15*, 2312–2323. https://doi.org/10.1091/mbc.e03-12-0913.

48. Akin, O., and Mullins, R.D. (2008). Capping protein increases the rate of actin-based motility by promoting filament nucleation by the Arp2/3 complex. Cell *133*, 841–851. https://doi.org/10.1016/j.cell.2008.04.011.

49. Reymann, A.-C., Suarez, C., Guérin, C., Martiel, J.-L., Staiger, C.J., Blanchoin, L., and Boujemaa-Paterski, R. (2011). Turnover of branched actin filament networks by stochastic fragmentation with ADF/cofilin. Mol. Biol. Cell *22*, 2541–2550. https://doi.org/10.1091/mbc.E11-01-0052.

50. Kawska, A., Carvalho, K., Manzi, J., Boujemaa-Paterski, R., Blanchoin, L., Martiel, J.-L., and Sykes, C. (2012). How actin network dynamics control the onset of actin-based motility. Proc. Natl. Acad. Sci. USA *109*, 14440–14445. https://doi.org/10.1073/pnas.1117096109.

51. Xu, M., Rutkowski, D.M., Rebowski, G., Boczkowska, M., Pollard, L.W., Dominguez, R., Vavylonis, D., and Ostap, E.M. (2024). Myosin-I synergizes with Arp2/3 complex to enhance the pushing forces of branched actin networks. Sci. Adv. *10*, eado5788. https://doi.org/10.1126/sciadv.ado5788.

52. Yamamoto, S., Gaillard, J., Vianay, B., Guerin, C., Orhant-Prioux, M., Blanchoin, L., and Théry, M. (2022). Actin network architecture can ensure robust centering or sensitive decentering of the centrosome. EMBO J. *41*, e111631. https://doi.org/10.15252/embj.2022111631.

53. Kandiyoth, F.B., and Michelot, A. (2023). Reconstitution of actin-based cellular processes: why encapsulation changes the rules. Eur. J. Cell Biol. *102*, 151368. https://doi.org/10.1016/j.ejcb.2023.151368.

54. Goehring, N.W., and Hyman, A.A. (2012). Organelle growth control through limiting pools of cytoplasmic components. Curr. Biol. *22*, R330–R339. https://doi.org/10.1016/j.cub.2012.03.046.

55. Marshall, W.F. (2020). Scaling of subcellular structures. Annu. Rev. Cell Dev. Biol. *36*, 219–236. https://doi.org/10.1146/annurev-cellbio-020520-113246.

56. Wang, Y.L. (1985). Exchange of actin subunits at the leading edge of living fibroblasts: possible role of treadmilling. J. Cell Biol. *101*, 597–602. https://doi.org/10.1083/jcb.101.2.597.

57. Theriot, J.A., and Mitchison, T.J. (1991). Actin microfilament dynamics in locomoting cells. Nature *352*, 126–131. https://doi.org/10.1038/352126a0.

58. Watanabe, N., and Mitchison, T.J. (2002). Single-molecule speckle analysis of actin filament turnover in lamellipodia. Science *295*, 1083–1086. https://doi.org/10.1126/science.1067470.

59. Wiesner, S., Helfer, E., Didry, D., Ducouret, G., Lafuma, F., Carlier, M.-F., and Pantaloni, D. (2003). A biomimetic motility assay provides insight into the mechanism of actin-based motility. J. Cell Biol. *160*, 387–398. https://doi.org/10.1083/jcb.200207148.

60. van Oudenaarden, A., and Theriot, J.A. (1999). Cooperative symmetry-breaking by actin polymerization in a model for cell motility. Nat. Cell Biol. *1*, 493–499. https://doi.org/10.1038/70281.

61. Dayel, M.J., Akin, O., Landeryou, M., Risca, V., Mogilner, A., and Mullins, R.D. (2009). In silico reconstitution of actin-based symmetry breaking and motility. PLoS Biol. *7*, e1000201. https://doi.org/10.1371/journal.pbio.1000201.

62. Colin, A., Orhant-Prioux, M., Guérin, C., Savinov, M., Cao, W., Vianay, B., Scarfone, I., Roux, A., De La Cruz, E.M., Mogilner, A., et al. (2023). Friction patterns guide actin network contraction. Proc. Natl. Acad. Sci. USA *120*, e2300416120. https://doi.org/10.1073/pnas.2300416120.

63. Strale, P.O., Azioune, A., Bugnicourt, G., Lecomte, Y., Chahid, M., and Studer, V. (2016). Multiprotein printing by light-induced molecular adsorption. Adv. Mater. *28*, 2024–2029. https://doi.org/10.1002/adma.201504154.

64. Luo, X., Seveau de Noray, V., Aoun, L., Biarnes-Pelicot, M., Strale, P.-O., Studer, V., Valignat, M.-P., and Theodoly, O. (2020). Lymphocytes perform reverse adhesive haptotaxis mediated by LFA-1 integrins. J. Cell Sci. *133*, jcs242883. https://doi.org/10.1242/jcs.242883.

65. Achard, V., Martiel, J.-L., Michelot, A., Guérin, C., Reymann, A.-C., Blanchoin, L., and Boujemaa-Paterski, R. (2010). A "primer"-based mechanism underlies branched actin filament network formation and motility. Curr. Biol. *20*, 423–428. https://doi.org/10.1016/j.cub.2009.12.056.

66. Manor, U., and Kachar, B. (2008). Dynamic length regulation of sensory stereocilia. Semin. Cell Dev. Biol. *19*, 502–510. https://doi.org/10.1016/j.semcdb.2008.07.006.

67. Littlefield, R.S., and Fowler, V.M. (2008). Thin filament length regulation in striated muscle sarcomeres: pointed-end dynamics go beyond a nebulin ruler. Semin. Cell Dev. Biol. *19*, 511–519. https://doi.org/10.1016/j.semcdb.2008.08.009.

68. Belyantseva, I.A., Perrin, B.J., Sonnemann, K.J., Zhu, M., Stepanyan, R., McGee, J., Frolenkov, G.I., Walsh, E.J., Friderici, K.H., Friedman, T.B., and Ervasti, J.M. (2009). γ-actin is required for cytoskeletal maintenance but not development. Proc. Natl. Acad. Sci. USA *106*, 9703–9708. https://doi.org/10.1073/pnas.0900221106.

69. Perrin, B.J., Sonnemann, K.J., and Ervasti, J.M. (2010). β-actin and γ-actin Are Each Dispensable for Auditory Hair Cell Development but Required for stereocilia Maintenance. PLoS Genet. *6*, e1001158. https://doi.org/10.1371/journal.pgen.1001158.

70. Zhang, D.-S., Piazza, V., Perrin, B.J., Rzadzinska, A.K., Poczatek, J.C., Wang, M., Prosser, H.M., Ervasti, J.M., Corey, D.P., and Lechene, C.P. (2012). Multi-isotope imaging mass spectrometry reveals slow protein turnover in hair-cell stereocilia. Nature *481*, 520–524. https://doi.org/10.1038/nature10745.

71. Colpan, M., Iwanski, J., and Gregorio, C.C. (2021). CAP2 is a regulator of actin pointed end dynamics and myofibrillogenesis in cardiac muscle. Commun. Biol. *4*, 365. https://doi.org/10.1038/s42003-021-01893-w.

72. Winkelman, J.D., Anderson, C.A., Suarez, C., Kovar, D.R., and Gardel, M.L. (2020). Evolutionarily diverse LIM domain-containing proteins bind stressed actin filaments through a conserved mechanism. Proc. Natl. Acad. Sci. USA *117*, 25532–25542. https://doi.org/10.1073/pnas.2004656117.

73. Phua, D.Y.Z., Sun, X., and Alushin, G.M. (2024). Force-activated zyxin assemblies coordinate actin nucleation and crosslinking to orchestrate stress fiber repair. bioRxiv. https://doi.org/10.1101/2024.05.17.594765.

74. Rotty, J.D., Wu, C., and Bear, J.E. (2013). New insights into the regulation and cellular functions of the Arp2/3 complex. Nat. Rev. Mol. Cell Biol. *14*, 7–12. https://doi.org/10.1038/nrm3492.

75. Chakrabarti, R., Lee, M., and Higgs, H.N. (2021). Multiple roles for actin in secretory and endocytic pathways. Curr. Biol. *31*, R603–R618. https://doi.org/10.1016/j.cub.2021.03.038.

76. Bieling, P., Li, T.-D., Weichsel, J., McGorty, R., Jreij, P., Huang, B., Fletcher, D.A., and Mullins, R.D. (2016). Force feedback controls motor activity and mechanical properties of self-assembling branched actin networks. Cell *164*, 115–127. https://doi.org/10.1016/j.cell.2015.11.057.

77. Boujemaa-Paterski, R., Suarez, C., Klar, T., Zhu, J., Guérin, C., Mogilner, A., Théry, M., and Blanchoin, L. (2017). Network heterogeneity regulates steering in actin-based motility. Nat. Commun. *8*, 655. https://doi.org/10.1038/s41467-017-00455-1.

78. Manhart, A., Icheva, T.A., Guerin, C., Klar, T., Boujemaa-Paterski, R., Thery, M., Blanchoin, L., and Mogilner, A. (2019). Quantitative regulation of the dynamic steady state of actin networks. Elife *8*, e42413. https://doi.org/10.7554/eLife.42413.

79. Li, T.-D., Bieling, P., Weichsel, J., Mullins, R.D., and Fletcher, D.A. (2022). The molecular mechanism of load adaptation by branched actin networks. Elife *11*, e73145. https://doi.org/10.7554/eLife.73145.

80. Reddien, P.W. (2024). The purpose and ubiquity of turnover. Cell *187*, 2657–2681. https://doi.org/10.1016/j.cell.2024.04.034.

81. Lewis, C.T.A., Melhedegaard, E.G., Ognjanovic, M.M., Olsen, M.S., Laitila, J., Seaborne, R.A.E., Grønset, M.N., Zhang, C., Iwamoto, H., Hessel, A.L., et al. (2024). Remodeling of skeletal muscle myosin metabolic states in hibernating mammals. Elife *13*, RP94616. https://doi.org/10.7554/eLife.94616.

82. Sagot, I., Pinson, B., Salin, B., and Daignan-Fornier, B. (2006). Actin bodies in yeast quiescent cells: an immediately available actin reserve? Mol. Biol. Cell *17*, 4645–4655. https://doi.org/10.1091/mbc.e06-04-0282.

83. Letort, G., Ennomani, H., Gressin, L., Théry, M., and Blanchoin, L. (2015). Dynamic reorganization of the actin cytoskeleton. F1000Res *4*, F1000. https://doi.org/10.12688/f1000research.6374.1.

84. Wales, P., Schuberth, C.E., Aufschnaiter, R., Fels, J., García-Aguilar, I., Janning, A., Dlugos, C.P., Schäfer-Herte, M., Klingner, C., Wälte, M., et al. (2016). Calcium-mediated actin reset (CaAR) mediates acute cell adaptations. Elife *5*, e19850. https://doi.org/10.7554/eLife.19850.

85. Lambert, C., Schmidt, K., Karger, M., Stadler, M., Stradal, T.E.B., and Rottner, K. (2023). Cytochalasans and their impact on actin filament remodeling. Biomolecules *13*, 1247. https://doi.org/10.3390/biom13081247.

86. Vedula, P., Kurosaka, S., MacTaggart, B., Ni, Q., Papoian, G., Jiang, Y., Dong, D.W., and Kashina, A. (2021). Different translation dynamics of β- and γ-actin regulates cell migration. Elife *10*, e68712. https://doi.org/10.7554/eLife.68712.

87. Vitriol, E.A., Wise, A.L., Berginski, M.E., Bamburg, J.R., and Zheng, J.Q. (2013). Instantaneous inactivation of cofilin reveals its function of F-actin disassembly in lamellipodia. Mol. Biol. Cell *24*, 2238–2247. https://doi.org/10.1091/mbc.E13-03-0156.

88. Liu, Y.-J., Le Berre, M., Lautenschlaeger, F., Maiuri, P., Callan-Jones, A., Heuzé, M., Takaki, T., Voituriez, R., and Piel, M. (2015). Confinement and low adhesion induce fast amoeboid migration of slow mesenchymal cells. Cell *160*, 659–672. https://doi.org/10.1016/j.cell.2015.01.007.

89. Lee, S., and Kumar, S. (2020). Cofilin is required for polarization of tension in stress fiber networks during migration. J. Cell Sci. *133*, 243873. https://doi.org/10.1242/jcs.243873.

90. Mertz, A.F., Banerjee, S., Che, Y., German, G.K., Xu, Y., Hyland, C., Marchetti, M.C., Horsley, V., and Dufresne, E.R. (2012). Scaling of traction forces with the size of cohesive cell colonies. Phys. Rev. Lett. *108*, 198101. https://doi.org/10.1103/PhysRevLett.108.198101.

91. Reinhart-King, C.A., Dembo, M., and Hammer, D.A. (2005). The dynamics and mechanics of endothelial cell spreading. Biophys. J. *89*, 676–689. https://doi.org/10.1529/biophysj.104.054320.

92. Rafelski, S.M., and Marshall, W.F. (2008). Building the cell: design principles of cellular architecture. Nat. Rev. Mol. Cell Biol. *9*, 593–602. https://doi.org/10.1038/nrm2460.

93. Kotila, T., Wioland, H., Enkavi, G., Kogan, K., Vattulainen, I., Jégou, A., Romet-Lemonne, G., and Lappalainen, P. (2019). Mechanism of synergistic actin filament pointed end depolymerization by cyclase-associated protein and cofilin. Nat. Commun. *10*, 5320. https://doi.org/10.1038/s41467-019-13213-2.

94. Suarez, C., Roland, J., Boujemaa-Paterski, R., Kang, H., McCullough, B.R., Reymann, A.-C., Guérin, C., Martiel, J.-L., De La Cruz, E.M., and Blanchoin, L. (2011). Cofilin tunes the nucleotide state of actin filaments and severs at bare and decorated segment boundaries. Curr. Biol. *21*, 862–868. https://doi.org/10.1016/j.cub.2011.03.064.

95. Almo, S.C., Pollard, T.D., Way, M., and Lattman, E.E. (1994). Purification, characterization and crystallization of Acanthamoeba profilin expressed in Escherichia coli. J. Mol. Biol. *236*, 950–952. https://doi.org/10.1006/jmbi.1994.1200.

96. Spudich, J.A., and Watt, S. (1971). The regulation of rabbit skeletal muscle contraction. I. Biochemical studies of the interaction of the tropomyosin-troponin complex with actin and the proteolytic fragments of myosin. J. Biol. Chem. *246*, 4866–4871. https://doi.org/10.1016/S0021-9258(18)62016-2.

97. Isambert, H., Venier, P., Maggs, A.C., Fattoum, A., Kassab, R., Pantaloni, D., and Carlier, M.-F. (1995). Flexibility of actin filaments derived from thermal fluctuations. Effect of bound nucleotide, phalloidin, and muscle regulatory proteins. J. Biol. Chem. *270*, 11437–11444. https://doi.org/10.1074/jbc.270.19.11437.

98. Egile, C., Loisel, T.P., Laurent, V., Li, R., Pantaloni, D., Sansonetti, P.J., and Carlier, M.-F. (1999). Activation of the Cdc42 effector N-wasp by the Shigella flexneri Icsa protein promotes actin nucleation by Arp2/3 complex and bacterial actin-based motility. J. Cell Biol. *146*, 1319–1332. https://doi.org/10.1083/jcb.146.6.1319.

99. Palmgren, S., Ojala, P.J., Wear, M.A., Cooper, J.A., and Lappalainen, P. (2001). Interactions with PIP2, ADP-actin monomers, and capping protein regulate the activity and localization of yeast twinfilin. J. Cell Biol. *155*, 251–260. https://doi.org/10.1083/jcb.200106157.

100. Schindelin, J., Arganda-Carreras, I., Frise, E., Kaynig, V., Longair, M., Pietzsch, T., Preibisch, S., Rueden, C., Saalfeld, S., Schmid, B., et al. (2012). Fiji: an open-source platform for biological-image analysis. Nat. Methods *9*, 676–682. https://doi.org/10.1038/nmeth.2019.

101. Ershov, D., Phan, M.-S., Pylvänäinen, J.W., Rigaud, S.U., Le Blanc, L., Charles-Orszag, A., Conway, J.R.W., Laine, R.F., Roy, N.H., Bonazzi, D., et al. (2022). TrackMate 7: integrating state-of-the-art segmentation algorithms into tracking pipelines. Nat. Methods *19*, 829–832. https://doi.org/10.1038/s41592-022-01507-1.

102. Pantaloni, D., Boujemaa, R., Didry, D., Gounon, P., and Carlier, M.-F. (2000). The Arp2/3 complex branches filament barbed ends: functional antagonism with capping proteins. Nat. Cell Biol. *2*, 385–391. https://doi.org/10.1038/35017011.

STAR★METHODS

KEY RESOURCES TABLE

REAGENT or RESOURCE	SOURCE	IDENTIFIER
Bacterial and virus strains		
BL21 (DE3) pLysS	Merck	Cat# 69451
Rosettas 2 (DE3) p Lys S	Merck	Cat# 71403
Biological samples		
Bovine Thymus	Slaughterhouse	
Rabbit Muscle Acetone powder	Pel-Freez Biologicals	Cat# 41995–2
Chemicals, peptides, and recombinant proteins		
Hellmanex III – Hellma Analytics	Sigma-Aldrich	Z805939-1EA
NOA 81 Norland Optical Adhesive 81 (Norland Products INC, PN 8101)	Thorlabs	NOA81
PDMS (Dow, SYLGARD 184 silicone elastomer kit)	Samaro	DE9330
Mineral oil (Paragon scientific Viscosity Reference Standard RTM13)	ThermoFisher Scientific	13536020
mPEG-Silane MW 30k	Creative PEGWorks	Cat# PSB-2014
Alexa Fluor 488 C5 Maleimide	ThermoFisher Scientific	Cat# A10254
Alexa Fluor 568 NHS Ester	ThermoFisher Scientific	Cat# A20003
Fluoresbrite BB Carboxylate 4.5 microns	Biovalley	18340-5
Polybead Carboxylate Microspheres 4.50 microns	Biovalley	17140-5
L-α-phosphatidylcholine (EggPC)	Avanti	840051C
DSPE-PEG(2000) Biotin (1,2-distearoyl-sn-glycero-3 phosphoethanolamine-N-[biotinyl(polyethylene glycol)-2000], ammonium salt	Avanti	880129C-10mg chloroform
ATTO 390 labeled DOPE (ATTO-TEC, AD 390-161 dehydrated)	Avanti	AD 390-161 dehydrated
Liquid PLPP Primo	Alveole	PLPP
Trichloro (1H,1H,2H,2H,perfluorooctyl) silane	Sigma Aldrich	448931
Methylcellulose (1500cP)	Sigma Aldrich	M0387
ATP	Sigma-Aldrich	A3377
DTT	Sigma-Aldrich	D9779
DABCO	Sigma-Aldrich	D27802
BSA	Sigma-Aldrich	A7030
Human Profilin 1 (Uniprot P07737)	This study	
Yeast cofilin (Uniprot Q03048)	This study	
Snap-Streptavidin-WA-His (Uniprot P42768)	This study	
Mouse Capping Proteins (a & b subunits, Uniprot P47754 and P47757)	This study	
Cyclase Associated Protein (Uniprot P40124)	This study	
Critical commercial assays		
HiPrep26/60 Sephacryl S-300 High resolution	Sigma-Aldrich	GE17-1196-01
HiLoad 16/60 Superdex 200 prep grade	Sigma-Aldrich	17-1069-01
Glutathione Sepharose 4B	Sigma-Aldrich	GE17-0756-05
HiTrap SP HP	Sigma-Aldrich	GE17-1151-01
Sephadex G-25	Sigma-Aldrich	G25150

(*Continued on next page*)

Continued

REAGENT or RESOURCE	SOURCE	IDENTIFIER
HisTrap HP	Cytiva	17524802
Recombinant DNA		
pET30a Snap-Strep-WA-His (Kanamycin resistance)	Colin et al.[43]	
pSUMOck4-MmCAP1(2-474) (Insert: Mouse CAP1 full length),kanamycin resistance	Kotila et al.[93]	pPL1358
pGEX GST-Yeast-cofilin1(D34C), carbenicillin resistance	Suarez et al.[94]	
pMW172 Human profilin1 (ampicilin resistance)	Almo et al.[95]	
pRFSDuet-1 His-Mouse Capping-Protein (α/β) (carbenicillin resistance)	Boujemaa-Paterski et al.[77]	
Software and algorithms		
Prism 10 (v10.1.0)	Graphpad Software	https://www.graphpad.com/scientificsoftware/prism/
Fiji	National Institutes of Health (Open Source Software)	https://fiji.sc
NIS-Elements	Nikon Instruments	https://www.microscope.healthcare.nikon.com/en_EU/products/software/nis-elements
R software (4.2.1)	R Foundation	https://cran.rstudio.com/
Other		
Coverglasses 20*20 mm n°1.5	VWR	630-2101
Superfrost Microscope Slides	VWR	631-0705

EXPERIMENTAL MODEL AND STUDY PARTICIPANT DETAILS

Protein purification

Actin was purified from rabbit skeletal-muscle acetone powder.[96] Monomeric Ca-ATP-actin was purified by gel-filtration chromatography on Sephacryl S-300 at 4°C in G buffer (2 mM Tris–HCl, pH 8.0, 0.2 mM ATP, 0.1 mM $CaCl_2$, 1 mM NaN_3 and 0.5 mM dithiothreitol (DTT)). Actin was labelled on lysines with Alexa-568.[97] All experiments were carried out with 5% labelled actin. The Arp2/3 complex was purified from calf thymus according to[78,98]. The Arp2/3 complex was purified from bovine thymus. Calf thymus was cut into approximately 1 cm pieces and mixed with extraction buffer (20 mM Tris pH 7.5, 25 mM KCl, 1 mM $MgCl_2$, 5% glycerol, protease inhibitors) for 1-2 minutes, then shaken in a beaker for 30 minutes. The extract was then centrifuged in a benchtop centrifuge at 1700×g for 5 minutes, and the supernatant clarified at 39,000×g for 25 minutes at 4°C. The supernatant was then filtered over glass wool, the pH was fixed at 7.5 with KOH and centrifugation was carried out at 140,000×g at 4°C for 1 hour. The medium aqueous phase was transferred to a chilled glass beaker, the extract was precipitated with 50% ammonium sulfate and centrifuged at 39,000×g for 30 minutes at 4°C. The pellet was resuspended in 10 mL extraction buffer with 0.2 mM ATP, 1 mM DTT and protease inhibitor. It was then dialyzed overnight in Arp2/3 dialysis buffer (20 mM Tris pH 7.5, 25 mM KCl, 1 mM $MgCl_2$, 5% glycerol, 1 mM DTT and 0.2 mM ATP). A GST-WA glutathione sepharose column was prepared and washed with extraction buffer containing 0.2 mM ATP, 1 mM DTT and protease inhibitors. The dialyzed extract was passed over the GST-WA column. Next, the column was washed with 20 mL extraction buffer with 0.2 mM ATP, 1 mM DTT and then with 20 mL extraction buffer with 0.2 mM ATP, 1 mM DTT and 100 mM KCl. The Arp2/3 complex was eluted with 20 mL extraction buffer with 0.2 mM ATP, 1 mM DTT and 200 mM $MgCl_2$, then dialyzed in source buffer A (piperazine-N,N′-bis(2-ethanesulfonic acid) (PIPES) pH 6. 8, 25 mM KCl, 0.2 mM ethylene glycol-bis(β-aminoethyl ether)-N,N,N′,N′-tetraacetic acid (EGTA), 0.2 mM $MgCl_2$ and 1 mM DTT) overnight. The Arp2/3 complex was then loaded onto a MonoS column and eluted with source buffer B (piperazine-N,N′-bis(2-ethanesulfonic acid) (PIPES) pH 6.8, 1 M KCl, 0.2 mM ethylene glycol-bis(β-aminoethyl ether)-N,N,N′,N′-tetraacetic acid (EGTA), 0.2 mM MgCl2 and 1 mM DTT). The Arp2/3 complex was dialyzed in storage buffer (10 mM Imidazole pH 7.0, 50 mM KCl, 1 mM $MgCl_2$, 0.2 mM ATP, 1 mM DTT and 5% glycerol), flash-frozen in liquid nitrogen and stored at -80°C. Human profilin was expressed in BL21 DE3 pLys *Escherichia coli* cells and purified according to.[95] Mouse capping protein was purified according to.[99] Briefly, Capping Protein was expressed in Rosetta2 DE3 pLys S in LB carbenicillin (100 μg/ml). Culture were grown until OD 600nm is 0.6 and induced with 0.5 mM IPTG at 26°C overnight. Cells were pelleted and resuspended in Buffer 1 (20 mM tris pH 8.0, 250 mM NaCl, 10mM Imidazole, 5% Glycerol, 1 mM DTT, 1 mM EDTA) + protease inhibitors cocktail tablet. Cells were sonicated and centrifuged at 16 000 rpm in a JA20 beckman rotor. Supernatant was applied to 1 mL of Ni sepharose fast flow resin (GE healthcare). After one hour at 4°C under gentle rotation, resin was washed with 20 volumes of Buffer 1 containing 50

mM Imidazole. Elution was performed with buffer 1+ 300 mM Imidazole. Purified protein was dialysed over night against a storage buffer (20 mM Tris pH 8.0, 1 mM DTT, 1 mM EDTA, 0.2 mM $CaCl_2$), flash frozen in liquid nitrogen and stored at -80°C. Yeast cofilin was purified and fluorescently-labelled according to.[94] Briefly, D34C mutant *S. cerevisiae* ADF/cofilin was expressed in Escherichia coli strain Rosetta2(DE3)pLysS and purified. The D34C mutant ADF/cofilin was then labeled on Cys34 with Alexa-488 C5Maleimide as follow: ADF/cofilin was dialysed in 10 mM Tris pH 8, 150 mM NaCl, 2 mM EDTA, 2 mM TCEP, incubated with 8 excess of Alexa-488 C5 Maleimide for two hours at 4°C, and separated on a Sephadex G-25 gel filtration column. Labeled ADF/cofilin was flash frozen in liquid nitrogen and stored in buffer (10 mM Tris pH 8, 150 mM NaCl, 2 mM EDTA, 2 mM DTT) at -80°C. The full-length mouse cyclase associated protein 1 (CAP1) was purified in a similar fashion as described in [93]. To describe briefly, the CAP1 protein was expressed in *E.coli* cells (Sigma) in LB medium at +16°C for 30 hours. The bacteria were pelleted and resuspended to buffer A (50 mM Tris pH 7.5, 150 mM NaCl, 25 mM imidazole) and lysed by sonification in the presence of protease inhibitors (200 μg/ml PMSF, 1 μg/ml leupeptin, 1 μg/ml aprotinin, 1 μg/ml pepstatin A, 150 μg/ml benzamidine hydrochloride, all from Sigma-Aldrich). The supernatant, clarified by centrifugation, was then loaded to a 5 mL HisTrap Ni-NTA column coupled to AKTA Pure protein purification system (GE Healthcare). The His-SUMO-tagged CAP1 protein was eluted from the nickel column with an imidazole gradient using buffer A and buffer B (buffer A + 250 mM imidazole), and the main peak fractions were collected and concentrated with Amicon Ultra-15 30 kDa cutoff centrifugal filter device. The His-SUMO-tag was then cleaved from the CAP protein in the presence of SENP2 protease, after which the cleaved protein was subjected to gel filtration runs by using Superose 6 increase 10/300 GL gel filtration column equilibrated in 5 mM HEPES, 100 mM NaCl, 1 mM DTT, 1 μg/ml leupeptin, pH 7.4. Peak fractions from the same elution volume were combined, concentrated as above and snap-frozen with liquid N_2 for long term storage at -75°C. Snap-Streptavidin-WA-His was purified as described in.[43] Snap-Streptavidin-WA-His (pETplasmid) was expressed in Rosetta 2 (DE3) pLysS (Merck, 71403). Culture was grown in TB medium supplemented with 30 μg/mL kanamycine and 34 μg/mL chloramphenicol, then 0.5 mM IPTG was added and protein was expressed overnight at 16 °C. Pelleted cells were resuspended in Lysis buffer (20 mM Tris pH8, 500 mM NaCl, 1 mM EDTA, 15 mM Imidazole, 0,1% TritonX100, 5% Glycerol, 1 mM DTT). Following sonication and centrifugation, the clarified extract was loaded on a Ni Sepharose high performance column (GE Healthcare Life Sciences, ref 17526802). Resin was washed with Wash buffer (20 mM Tris pH8, 500 mM NaCl, 1 mM EDTA, 30 mM Imidazole, 1 mM DTT). Protein was eluted with Elution buffer (20 mM Tris pH8, 500 mM NaCl, 1 mM EDTA, 300 mM Imidazole, 1 mM DTT). Purified protein was dialyzed overnight 4°C with storage buffer (20 mM Tris pH8, 150 mM NaCl, 1 mM EDTA, 1 mM DTT), concentrated with Amicon 3KD (Merck, ref UFC900324) to obtain concentration around 10 μM then centrifuged at 160,000 x g for 30 min. Aliquots were flash frozen in liquid nitrogen and stored at −80 °C.

Polystyrene beads coating

Polystyrene beads coating with NPF was done following classical protocols.[49] 20 μL of 4.5 μm polystyrene beads (Fluoresbrite BB Carboxylate Microspheres, 2.5% solids) were centrifuged at 13, 000 g for 2 minutes on a mini spin plus Eppendorf centrifuge (Rotor F45-12-11). The pellet was then resuspended in 200 μL of a 400 nM or 200 nM Snap-Streptavidin-WA-His solution. Beads were incubated for 15 minutes at 15°C at 950 rpm in a thermoshaker. They were then centrifuged for 2 minutes at 3800 g, resuspended in 200 μL of BSA 1% and let on ice for 5 minutes. Beads were finally centrifuged again 2 minutes at 3800 g and resuspended in 50 μL of BSA 0.1%. The bead coating was redone every day.

Estimation of protein density on beads

For a coating with 400 nM of NPF, we estimate that we have about 7,6 NPF molecule per 100 nm^2. Therefore, for a coating with 200 nM of NPF, this represents about 3,8 NPF molecule per 100 nm^2. These number are in the same order of magnitude as the conditions used in.[59]

Microwells preparation

Microwells used in this study have a diameter of 100 μm and a height of 40 μm, giving them a volume of about 314 pL. SU8 mold with pillars was prepared using standard protocols and silanized with Trichloro(1H,1H,2H,2H-perfluoro-octyl)silane for 1 hour and heated for 1 hour at 120°C. From the SU8 mold, a PDMS primary mold was prepared (Dow, SYLGARD 184 silicone elastomer kit) with a 1:10 w/w ratio of curing agent. PDMS was cured at 70°C for at least 2 hours. PDMS primary mold was then silanized with Trichloro(1H,1H,2H,2H-perfluoro-octyl)silane for 1 hour and heated for 2 hours at 100°C. PDMS was then poured on top of the PDMS primary mold to prepare the PDMS stamps.

Coverslips were cleaned with the following protocol: they were first wiped with ethanol (96%) then sonicated 30 minutes in Hellmanex 2% at 60°C. After the sonication, coverslips were rinsed in several volumes of mqH_2O and kept in water until use. Just before use, coverslips were dried with compressed air.

For the microwells preparation, PDMS Stamps were cut in pieces and placed on the coverslips with the pillars facing the coverslip. A drop (5 μL) of NOA 81 (Norland Products) was then placed on the side of the PDMS stamp and NOA was allowed to go through the PDMS Stamp by capillarity. When the NOA filled all the stamp, it was polymerized with UV light for 12 minutes (UV KUB2/ KLOE; 100% power). After polymerization of the NOA, PDMS stamp was removed and the excess of NOA was cut. Then, an additional UV exposure of 2 minutes was done and the microwells were placed on a hot plate at 110°C for at least 3 hours (or at 60°C overnight) to tightly bind the NOA to the glass.

Lipids/SUV preparation

For regular microwell passivation, L-α-phosphatidylcholine (EggPC) (Avanti, 840051C, 10 mg/mL) was used. The SUV were prepared as following: 100 μL of lipids were introduced in a glass tube and the mixture was dried with nitrogen gas. The dried lipids were incubated in a vacuum overnight. After that, the lipids were hydrated in the SUV buffer (10 mM Tris (pH 7.4), 150 mM NaCl, 2 mM $CaCl_2$). The mixture was sonicated on ice for 10 minutes. The mixture was then centrifuged for 10 min at 20,238 x g to remove large structures. The supernatants were collected, stored at 4°C and used for up to 3 weeks.

For the lipids used for the micropatterning, same protocol was used. The lipid mix was composed of L-α-phosphatidylcholine (EggPC) (Avanti, 840051C), DSPE-PEG(2000) Biotin (1,2-distearoyl-sn-glycero-3 phosphoethanolamine-N-[biotinyl(polyethylene glycol)-2000], ammonium salt, Avanti, : 880129C-10mg chloroform) and ATTO 390 labeled DOPE (ATTO-TEC, AD 390-161 dehydrated). Lipids were mixed in glass tubes as follows: 98.5% EggPC (10 mg/mL), 0.5% DSPE-PEG(2000) Biotin (10 mg/mL) and 1% DOPE-ATTO390 (1 mg/mL).

SilanePEG30k slides

SilanePEG (30kDa, PSB-2014, Creative PEG works) was prepared at a final concentration of 1 mg/mL in 96% ethanol and 0.1%(v/v) HCl. Slides were cleaned with the following protocol: they were sonicated for 30 minutes at 60°C in Hellmanex 2%. They were then rinsed with several volumes of mqH_2O and dried with compressed air. Slides were then plasma cleaned for 5 minutes at 80% power and directly immersed in the silanePEG solution. They were kept in the silanePEG solution until use.

Bead motility assay in microwells

A typical experiment of bead motility in microwells was performed as follows. The coverslip with microwells was activated with plasma for 2 minutes at 80% power. Just after the plasma, the flow chamber was mounted with the microwells coverslip, a slide passivated with SilanePEG 30k and 180 μm height double-side tape. Lipids were then inserted in the flow chamber and incubated for 10 minutes. Lipids were then rinsed with 1 mL of SUV buffer and 200 μL of 1x HKEM buffer (50 mM KCl, 15 mM HEPES pH=7.5, 5 mM $MgCl_2$, 1 mM EGTA). The reaction mix with the different proteins was then prepared and flowed in the flow cell.

A typical reaction mix (60 μL) was prepared with beads coated with WA (activator of the Arp2/3 complex) and 6 μM of actin monomers, 12 μM profilin, 90 nM Arp2/3 complex, 40 nM Capping Protein in HKEM Buffer and was supplemented with 0.7% BSA, 0.2% methylcellulose, 2.7 mM ATP, 5 mM DTT, 0.2 mM DABCO (motility buffer). When needed the polymerization mix was also supplemented with yeast cofilin and/or cyclase associated protein (CAP). The microwells were then closed with mineral oil (Paragon scientific Viscosity Reference Standard RTM13). The whole flow cell was then sealed with VALAP and directly imaged under the microscope.

Micropatterning in microwells

Micropatterning in microwells is done with the Primo device (Alveole). Prior to micropatterning, the microwells were activated with plasma for 5 minutes at 80% power and directly immersed in a SilanePEG (30k, cf section above) solution overnight. They were rinsed with ethanol and water just before use. A flow chamber was then built with the microwells and a slide passivated with SilanePEG with a double-side tape of 250 μm. Liquid photo initiator (PLPP) was then introduced in the flow chamber. Patterns were designed in Inkscape and loaded into the μmanager's Leonardo plugin (Alveole). The burning was done at 90 mJ at 100% of a 5.6 mW 365 nm wavelength laser. The flow chamber was then rinsed with 1 mL of water and 400 μL of SUV Buffer to remove the PLPP. 80 μL of SUV solution was then added and incubated for 10 minutes at room temperature for an effective lipid coating. The excess of SUV was washed out by passing 400 μL of SUV Buffer and 200 μL of 1x HKEM. The flow chamber was then passivated with 200 μL of 0,1% BSA diluted in 1x HKEM for 2 minutes and then rinsed with 400 μL of 1x HKEM. The NPF (Snap-Streptavidin-WA-His, 50 nM diluted in 1x HKEM and 0,1% BSA) was then injected in the flow chamber and the coating was done by letting incubate for 10 minutes at room temperature. The excess of NPFs was washed out by passing 1 mL of 1x HKEM. The reaction mix was then introduced (60 μL) and the microwells were subsequently closed with oil.

Imaging

Most of the experiments were done with an epifluorescence system (Ti2 Nikon inverted microscope equipped with a Hamamatsu Orca Flash 4.0 LT Plus Camera). The following objectives were used: Plan Fluor 10X DIC and S Plan Fluor ELWD 20X DIC. Time lapse were acquired with the NIS elements software (version 4.60).

Z-stacks of actin networks grown on micropatterns in microwells were performed with a confocal spinning-disc system (EclipseTi-E Nikon inverted microscope equipped with a CSUX1-A1 Yokogawa confocal head, an Evolve EMCCD camera (Photometrics), and a Plan Fluor 40X objective). Z-stacks were acquired with Metamorph software (Universal Imaging). Three-dimensional reconstructions were performed with the UCSF Chimera package. Chimera is developed by the Resource for Biocomputing, Visualization, and Informatics at the University of California (San Francisco) with support from the National Institutes of Health (National Center for Research Resources grant 2P41RR001081, National Institute of General Medical Sciences grant 9P41GM103311).

QUANTIFICATION AND STATISTICAL ANALYSIS

Image analysis

Images were analyzed with customed macros written in FiJi.[100] Data were then processed with R software and plotted with GraphPad Prism. Mean and standard deviation are represented for all the data. The dot plots show the individual values with the mean and standard deviation superimposed. Fits, calculation of correlation coefficient and statistical tests were done with GraphPad Prism. All the statistical information regarding replicates values can be found in figure legends.

Characterization of structure size for beads experiments

Actin comets were detected with the following procedure. First, threshold was adjusted manually and images were binarized. Actin comet area was obtained from the results of the Analyze particles function. Comet length was obtained with the ''skeletonize'' and ''analyze skeleton'' functions. Tracking of comets and fluorescent beads was then done with the TrackMate plugin using the thresholding or LoG detectors respectively.[101] In order to reduce experimental noise, the various quantities measured were averaged over one hour. For conditions without turnover, they were averaged between 200 and 260 minutes (dashed box, Figure 1C). For conditions with turnover, they were averaged between 120 and 180 minutes (dashed box, Figure 2C).

Characterization of structure size for micropatterns experiments

For experiments performed with micropatterns, since networks are growing in 3D, the area of the actin structure grown from the micropattern is more complicated to estimate. This is why we quantified the total quantity of actin polymerized from the micropattern. Similar to the analysis done for the beads, we used a thresholding of the fluorescence image of the actin channel. We then applied the Analyze particles function to the thresholded image to get ROIs of actin network grown on each pattern. We then measured the total actin intensity in the ROIs corresponding to each pattern that we report as Quantity of actin polymerized (in arbitrary units).

Estimation of the ratio of actin consumed from bulk in the comet tail

To estimate the total quantity of actin in the microwell, we estimated the total fluorescence intensity. This value was constant during the time course of an experiment showing that the actin in the microwell is constant during an experiment. The quantity of actin inside a comet tail was estimated after thresholding and binarization of the comet. Those two fluorescence intensities were corrected for the fluorescence background. Then, we estimated the ratio of actin consumed from the bulk in the comet by computing the comet fluorescence over the total fluorescence of the microwell. We then came back to an actin concentration by considering that total fluorescence of the microwell corresponds to the initial amount of actin introduced in the microwell. The estimated bulk actin concentration is approximately 2 μM, which exceeds the critical concentration for barbed-end assembly (0.1 μM). This indicates the presence of a fraction of actin in the bulk solution within the microwell, contributing to additional competition for the growth of branched structures on the beads.

Estimation of protein quantity in microwells and of their consumption in experiments

We estimated the protein quantity in the microwells used in this study (Diameter of 100 μm, height of 40 μm, which gives a volume of 314 pL), Figure S1C. Following the same logic as the estimation we made in our previous study[43]: about 60% of the initial actin amount is polymerized (in conditions without turnover) which represents $6.6e^8$ monomers polymerized. Therefore, total length of all filaments polymerized is $6.6e^{8}*2.7 = 1{,}7e^6$ μm (2.7 nm being the size of an actin monomer). Mean filament length is around 300 nm so we have about $5.7e^6$ filaments and we consider that there is one Arp2/3 complex and one capping protein per filament. We found that about 33% of the Arp2/3 complex available is consumed in the comet tails, indicating that a global depletion of the Arp2/3 complex is unlikely. In addition, about 76% of Capping protein is consumed in the comet tails. However, as we do not see fishbone patterns appearing on the comet tails as a function of time,[102] we conclude that capping protein is not limiting in the assay. Therefore, we conclude that neither the Arp2/3 complex nor the capping protein is significantly limiting under our experimental conditions (Figure S1C).